Hindawi
International Journal of Aerospace Engineering
Volume 2019, Article ID 4014120, 22 pages
https://doi.org/10.1155/2019/4014120

Research Article

Flow Characteristics of a Rich-Quench-Lean Combustor-Combined Low-Emission and High-Temperature Rise Combustion

Jianzhong Li,[1] **Jian Chen**,[1] **Li Yuan**,[2] **Ge Hu**,[1] **and Jianhan Feng**[1]

[1]*Key Laboratory of Aero-engine Thermal Environment and Structure, Ministry of Industry and Information Technology, Nanjing University of Aeronautics and Astronautics, 29 Yudao St., Nanjing 210016, China*
[2]*School of National Defense Engineering, The Army Engineering University of PLA, 88 Biaoying Rd., Nanjing, 210007 Jiangsu, China*

Correspondence should be addressed to Jianzhong Li; ljzh0629@nuaa.edu.cn

Received 4 September 2018; Accepted 8 November 2018; Published 11 February 2019

Academic Editor: Jose Carlos Páscoa

To determine the flow field structure and flow characteristics of a rich-quench-lean (RQL) combustor-combined low-emission and high-temperature rise combustion, a two-dimensional PIV technology was used to evaluate the effect of aerodynamic and structural parameters on the flow field and flow characteristics of the combustor. The variation in the total pressure loss of the combustor has little effect on the flow field structure of the combustor. However, the variation in the parameters of primary holes significantly affects the structure of the central recirculation zone, the distribution of local recirculation zones in the rich-burn zone and quenching zone, and the average residence time in the quenching zone. On the plane that passes through the center of the primary hole, the variations in the array mode and diameter of primary holes would form entrainment vortexes with different characteristics, thus affecting the position and flow state of local recirculation in the rich-burn zone and the local structure of the central recirculation zone. As the rotational direction of local recirculation coincides with that of the main air flow in the primary zone, the local center recirculation is intensified. In contrast, it is weakened. As the primary holes are located at half height (H/2) of the combustor, the residence time of air flow at the quenching zone can be shortened by 65% through using the staggered structure of primary holes and increasing the momentum of the partial single-hole jet. The quick-mixing process in the quenching zone is not beneficial to increase the number of primary holes and decrease the momentum of the single-hole jet.

1. Introduction

There are two straightforward and effective methods for improving the performance of a gas turbine engine. One is increasing the engine pressure ratio to raise the thermal efficiency, the other is increasing the outlet temperature of a combustor to raise the specific thrust. Therefore, the combustor of a gas turbine engine will be developed in the directions of high temperature rise and high heat capacity [1–3] and the design requirements for a combustor become stricter, such as a wider working range, shorter length, and smaller distribution parameter of outlet temperature. Simultaneously, the combustor is required to have a longer life and lower pollutant emission [4, 5].

In the early development of combustors with a high temperature rise, the design idea is only an increase in the fuel supply and change in the flow rate distribution without changing the structure of a conventional combustor to increase the combustor temperature rise. However, this mothed would cause a sharp increase in the exhaust and smoke of a combustor and obvious decrease of the stable working range [6]. Therefore, to satisfy the technical requirements of future combustors with high temperature rise, the conventional design concept of a combustor should be changed. It is necessary to further optimize the combustion organization, adjust the combustor flow rate distribution, and introduce an advanced cooling technology [7–10]. RQL combustion technology is a special staged combustion method. The initial zone is a fuel-rich combustion grade, the middle zone is a quenching grade, and the final zone is a lean-burn grade [11–14]. Because the initial zone is fuel-rich combustion with a relatively higher

equivalence ratio and lower flow rate, the combustor stable working range is relatively wider and has a better ignition performance. In the quenching stage, a large amount of air is introduced to perform a quick mixing with the burned gas in the primary zone, thereby completing the transient transition from the rich-burn zone to the lean-burn zone and preventing the rapid formation of thermal NOx at the stoichiometric ratio. In the lean-burn zone, high temperature rise and low pollutant emissions can be achieved to satisfy the design requirements by selecting an appropriate equivalence ratio. Therefore, the RQL combustion technology has been applied to the design of a combustor to achieve a reasonable combination of combustion with high temperature rise and low emission. For the application of low-heat value fuel and integrated gasification combined cycle, the General Electric Company successfully developed a full-scale industrial-grade RQL combustor using partitioned independent air intake [15]. The combustor outlet temperature reaches 1672 K, and the NOx emission decreases by ~3% compared with that of the conventional diffusion combustion using the same fuel. However, the combustor developed still uses the structure of a traditional RQL combustor and the fuel/air ratio range between the rich-burn zone and lean-burn zone is larger. To maintain higher combustion efficiency, it is inevitable to extend the length of the combustor middle zone. This is contrary to the trend of modern combustor development into a shorter ring. In addition, with the further requirement of the outlet temperature of the modern combustor, especially when the outlet temperature is as high as 1973 K, rapid mixing within the quenching zone is more difficult, i.e., the RQL combustion technology faces severe challenges [16]. Therefore, this is a new subject to effectively apply the RQL combustion technology in the design of modern combustors with a high temperature rise through a reasonable flow distribution and aerodynamic design.

The air flow enters the combustor through the jet orifice and dome vortex. Therefore, it exhibits a complex flow state by combining swirl and lateral jet. Simultaneously, there is an interaction between the swirl and jet. This has a crucial effect on the stable working range, the outlet temperature distribution, and the pollutant emission for a combustor [17, 18]. Therefore, a good aerodynamic layout is the design basis of modern combustors. The development of modern high-precision noncontact measurement technology provides favorable support for the study of combustor aerodynamic performance and optimization of its performance [19–27]. Richards and Samuelsen found that the position of the primary holes is critical to combustion and proposed that the axial position of primary holes should be 0.5-1 times the diameter of the round pipe to achieve the best matching with the mainstream [28, 29]. Mohammad et al. used a PIV system to study the interaction between the primary hole jet, the fuel injection, and the swirl. The effect of interaction on the combustor aerodynamic performance was evaluated [30]. Gogineni studied the effect of the primary holes on the characteristics of the primary zone. It was found that not only the pollutant was effectively reduced but also the flame length was shortened and the lean blowout performance was improved, as the axial positions of primary holes were at the half height of the combustor and the layout was up-down symmetrical [31]. Elkady et al. used a PIV system to study the effect of the axial position of the primary holes and the flow rate variation on the flow field structure and shape and size of the recirculation zone, and the mechanism that affects the combustor pollutant emission was elucidated [32]. Although these studies have laid an important theoretical foundation to improve the aerodynamic layout of conventional combustors and optimize the organization of combustion, they are not fully applicable to RQL combustion technology. In the design of a conventional combustor, the air amount involved in combustion increases due to the increasing of the temperature rise of a combustor, with the most obvious manifestation that the intake air amount through the combustor dome continuously increases. In the RQL combustion technology, however, a rapid uniform mixing in the quenching zone and the shortening of residence time are the key factors in the reduction of pollutant generation. To achieve the goal, the most effective way is to increase the momentum flux ratio between the hole jet and mainstream in the quenching zone and to increase the flow ratio of the quenching hole jet and mainstream to some extent [33]. To apply the RQL combustion technology to the design of a combustor with high temperature rise, the primary hole jet should be quickly and evenly mixed with the burned gas in the quenching zone. On the other hand, it is necessary to strengthen the combustion in the fuel-rich area and simultaneously perform supplemental combustion for the unburned mixture in the fuel-rich zone. If the ratio of the primary hole jet to the dome flow is too large (the conventional value of the RQL combustor is ~2.5), the dissociated product will freeze and inhibit the composite reaction. This is not conducive to the supplementary combustion of the combustible mixture and results in lower combustion efficiency. The two small flow rate ratios between the primary hole jet and dome flow (the value of conventional combustor is ~0.25) is not conducive to the rapid and uniform mixing in the quenching zone [34, 35]. Therefore, a good aerodynamic layout of a combustor through reasonable flow rate distribution and design of structure of primary holes would be achieved, which is the key to the successful application of RQL combustion technology in the design of a combustor with high temperature rise.

In this study, the RQL combustion technology was combined with the design of a high-temperature rise combustor and a single-dome rectangular combustor model was used. Under ambient temperature and pressure, the flow rate and equivalence ratio distribution are maintained according to a certain proportion (dome: 31% and 1.2, primary holes: 22% and 0.8, and dilution holes: 47% and 0.47) and the axial positions of the primary holes and the structural parameters of the dilution holes are unchanged. Using the two-dimensional (2D) PIV technology, the RQL combustor with high temperature rise was investigated.

2. Experimental Rig of the RQL Combustor with High Temperature Rise

The experimental rig of the RQL combustor with high temperature rise includes an air supply system, a measurement

system for total pressure, a laser generator, a digital camera, and a combustor [35]. The airflow is supplied by a Roots blower and divided into five branches (dome, upper primary holes and bottom primary holes, and upper dilution holes and bottom dilution holes) after passing through the main route. Each branch road is equipped with vortex flow meters and valves. The total inlet pressure was measured by installing a total pressure pipe. The valve on the branch was regulated to ensure the total inlet pressure of each inlet zone to satisfy the test conditions. Then, the flow rate of airflow was recorded and the flow field was measured by a PIV system. Taking the total pressure loss of the combustor dome as a reference, the total inlet pressures of the upper primary holes and the bottom primary holes and the dilution holes were consistent with the total inlet pressure of the combustor dome. The MgO particles with an average diameter of 10 μm were used as the tracing particle because of a sufficiently high followability. The tracing particles were emitted by a self-made particle generator and injected into the manifold. The particles moved along the air flow and entered the combustor through each intake branch. The axial distances between the injection position of tracing particles and each inlet of the combustor are more than 3 m. Therefore, there is sufficient mixing distance for tracing particles and airflow before the particles enter the combustor, ensuring the uniformity of tracer particle distribution in the combustor. To satisfy the requirements of optical measurement, a 150 mm × 65 mm observation window was opened at the combustor side wall and a quartz glass was mounted. Another observation window was installed at the combustor downstream outlet with an area equal to the combustor outlet (100 mm × 65 mm), and the exhaust burned gas was discharged through the side exhaust duct. A Nd:YAG double-pulse laser with a single-pulse maximum energy of 200 mJ, a laser wavelength of 532 nm, and a maximum operating frequency of 15 Hz was used in the test. The digital camera (Bobcat B2041, IMPERX) had a maximum resolution of 2048 × 2048 pixels, a minimum span time of 200 ns, and a maximum shooting frequency of 20 Hz. The synchronization controller (MicroPulse model 725) can control the laser, digital camera, and image acquisition board by setting delay-trigger signals for timing.

During the PIV measurement, the selection of the double-exposure time interval is very important. Through the double exposure of the laser instrument, the digital camera obtains two flow field images with a time interval. Considering the variations in flow rate and flow field, the double-exposure time interval should be determined by the combustor flow characteristics [36]. A too large or too small time interval is not appropriate because the time interval should ensure that the displacement of tracing particles during this time interval can be recognized and the tracing particles do not escape the acquisition area. The actual timer interval was set as 5 μs according to the estimation of possible maximum speed of particles in the combustor. On the orthogonal grid, the PIV data processing was performed by using the fast Fourier transform cross-correlation method. Considering that the overlap ratio of the tracer in the query area is 50% and the maximum displacement is 15-20%, the final query window size was 32 × 32 pixels. The relative error of the software was less than 1%, and the correction rate on the vector was less than 30%.

The combustor is a rectangular structure established based on RQL combustion technology. The specific dimension is 300 mm × 100 mm × 65 mm, as shown in Figure 1. In order to facilitate the test piece assembly and parameter measurement, the combustor does not have an external casing. The air flow is separately supplied into each combustion functional zone which includes a rich-burn zone, quenching zone, and lean-burn zone, and the cooling structure is ignored. The primary holes and dilution holes are first opened on a plate with a thickness of 1 mm and then connected to the outlet of inlet cavity, thus satisfying the sealing requirements and easily replacing the primary holes and the dilution hole structure. The swirler is a two-stage oblique-cutting orifice structure, and the rotational directions are opposite. From the combustor dome to the downstream, the rotational direction of the first-stage oblique-cutting orifice is clockwise, while the rotational direction of the second-stage oblique-cutting orifice is counterclockwise. According to the axial positions of the primary holes and the dilution holes, the combustor is divided into each combustion functional zone. The rich-burn zone extends from the swirler exit to the central area of primary holes with a distance of 32.5 mm. The quenching zone extends from the center of primary holes to the center of dilution holes with a length of 31 mm. The lean-burn zone extends from the center of dilution holes to the combustor outlet region with a distance of 236.5 mm. The structural parameters of dilution holes are identical, and a three-hole symmetric arrangement is used, where the spacing is 40 mm and the diameter is 6.4 mm. The primary holes have three different structures, and the structural parameters were shown in [35]. The specific flow rate distributions in the combustor are as follows: 31% for the combustor dome, 22% for the primary holes, and 47% for the dilution holes. The equivalence ratio distributions in the combustor are as follows: 1.2 for the rich-burn zone, 0.8 for the quenching zone, and 0.47 for the lean-burn zone.

Under ambient temperature and pressure, the measured planes include $Z = 0$ mm (meridian plane), $Z = -15.5$ mm (the circumstantial outlet plane of the swirler), $X = 20$ mm, $X = 32.5$ mm (the central plane of primary holes), $X = 48$ mm (the central plane in the quenching zone), and $X = 63.5$ mm (central plane of dilution holes), as shown in Figure 2.

The dimensions of the observation window with an axial plane of 150 mm × 65 mm and circular plane of 100 mm × 65 mm were used for PIV photography. The photography frequency was 15 Hz, and 200 photographs were recorded for each working condition. The magnification was 2.6 pixels/mm.

3. Results and Discussion

On the $Z = 0$ mm plane in the combustor, the flow field structures under different total pressure loss and structural parameters of the primary holes are shown in Figure 3, where the solid black line represents the zero velocity line, i.e., the

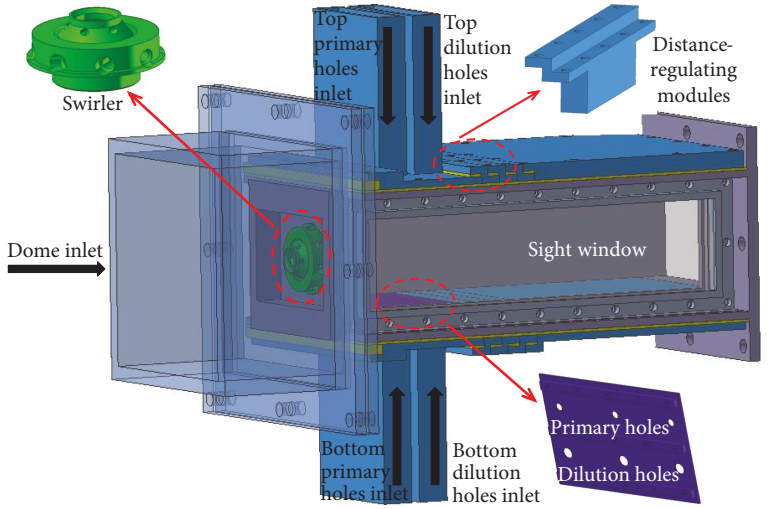

Figure 1: Geometry of the combustor model.

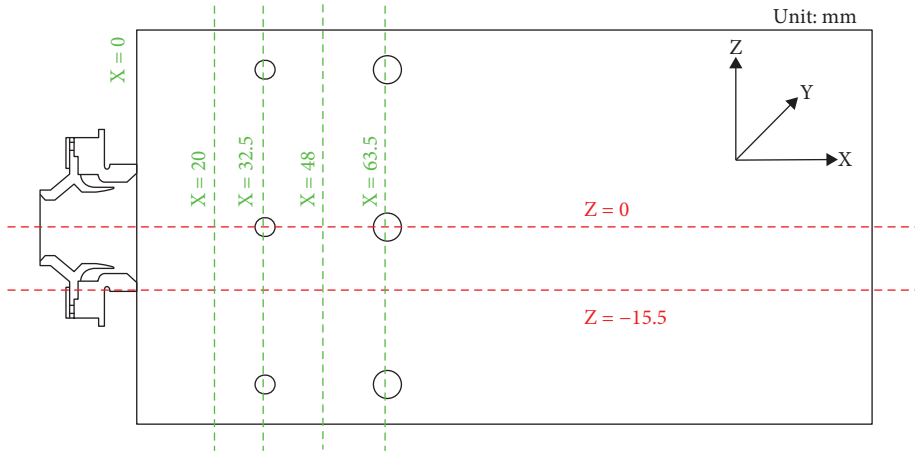

Figure 2: Sketch of the measurement plane for the PIV test.

boundaries of the recirculation zone. For a combustor model only with the dome air intake and without the jets obtained from the primary holes and the dilution holes (referred to as a nonjet combustor model), the dome air flow rotates after passing through the swirler. Under the action of centrifugal force, the central pressure decreases and creates a reverse pressure gradient. This forces the external airflow back to form a central recirculation zone. The air flow exhibits a forward flow outside the boundary line of the recirculation zone, whereas the air flow exhibits a reverse flow inside the boundary line. The air flow near the swirler exit has a larger axial and tangential momentum, and the momentum gradually decreases in the downward movement due to aerodynamic resistance. The back pressure gradient gradually decreases, and the height of the central recirculation zone first increases and then decreases. As the central recirculation zone expands, the flow zone of forward air flow gradually decreases. The flow velocity gradually increases, and the reverse velocity gradient in the recirculation zone increases. Thus, symmetrical recirculation zones with opposite rotational directions are formed at the highest boundary of the central recirculation zone. Limited by the dimension of the viewing window, the length of the central recirculation zone exceeds the observation window (150 mm). However, the boundary height of the recirculation zone at the tail ($X = 150$ mm) showed that the heights are ~15 mm, 16 mm, 18 mm, and 21 mm, indicating that the length of the central recirculation zone extends slightly with the increase in total pressure loss. With the introduction of jets from the primary holes and the dilution holes, the flow characteristics of the same model including the structure of the central recirculation zone, the forming position of the local recirculation zone, the jet trajectory, the jet position, and the structure of the tailing area are identical even though the flow field structures of three combustor models are distinctly different. The results show that the jets of primary holes and the dilution holes intensify the turbulence intensity in the combustor and all the flows in the three combustor models are in the self-modeling state with a flow field structure independent of the total pressure loss. The jet depth of the primary holes

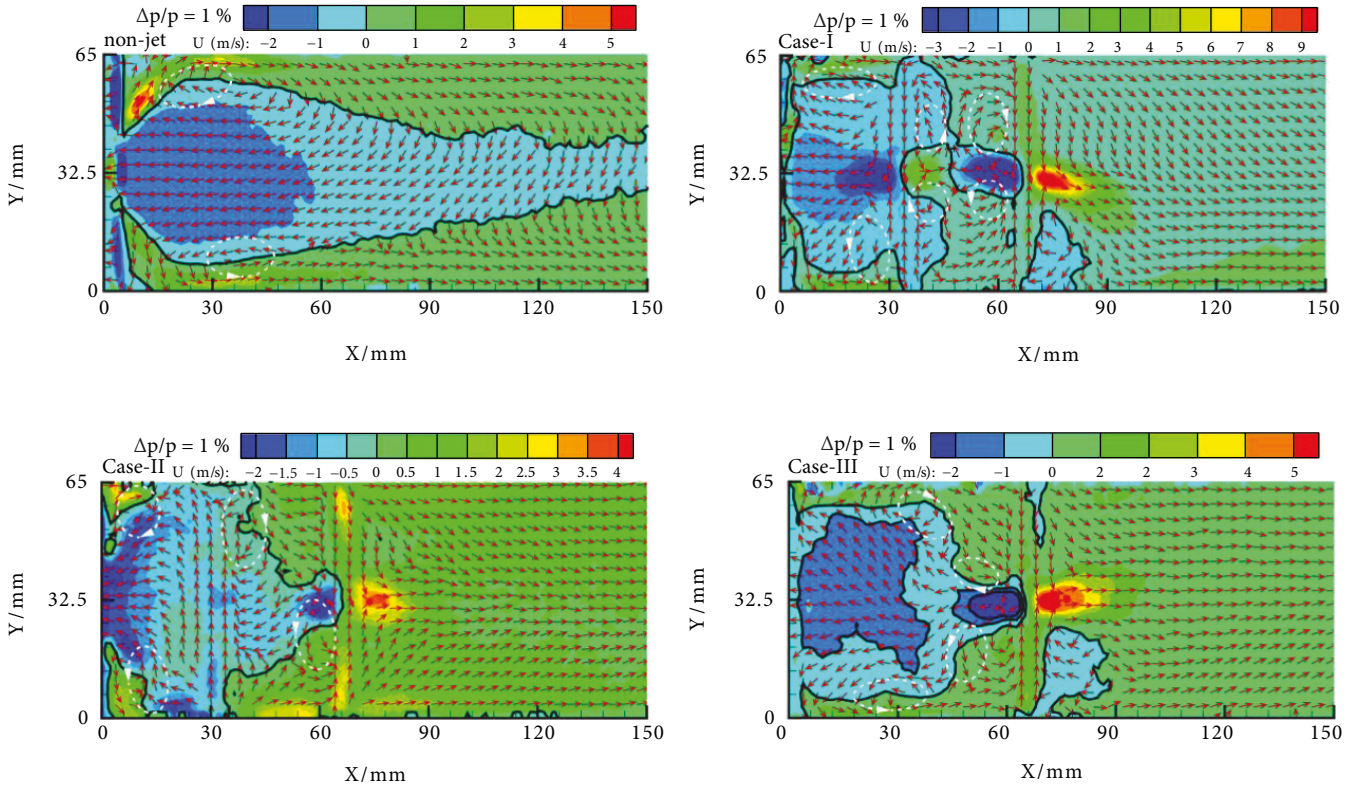

(a) Total pressure loss coefficient of 1%

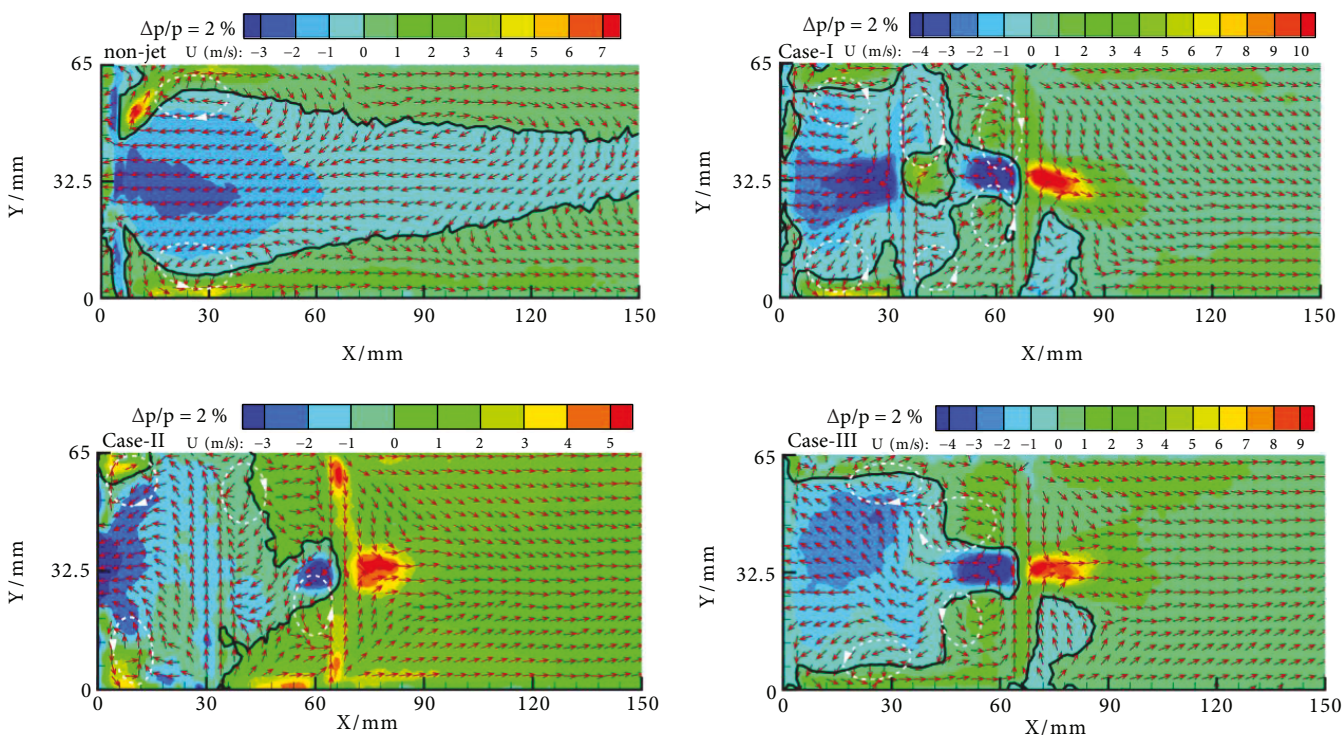

(b) Total pressure loss coefficient of 2%

Figure 3: Continued.

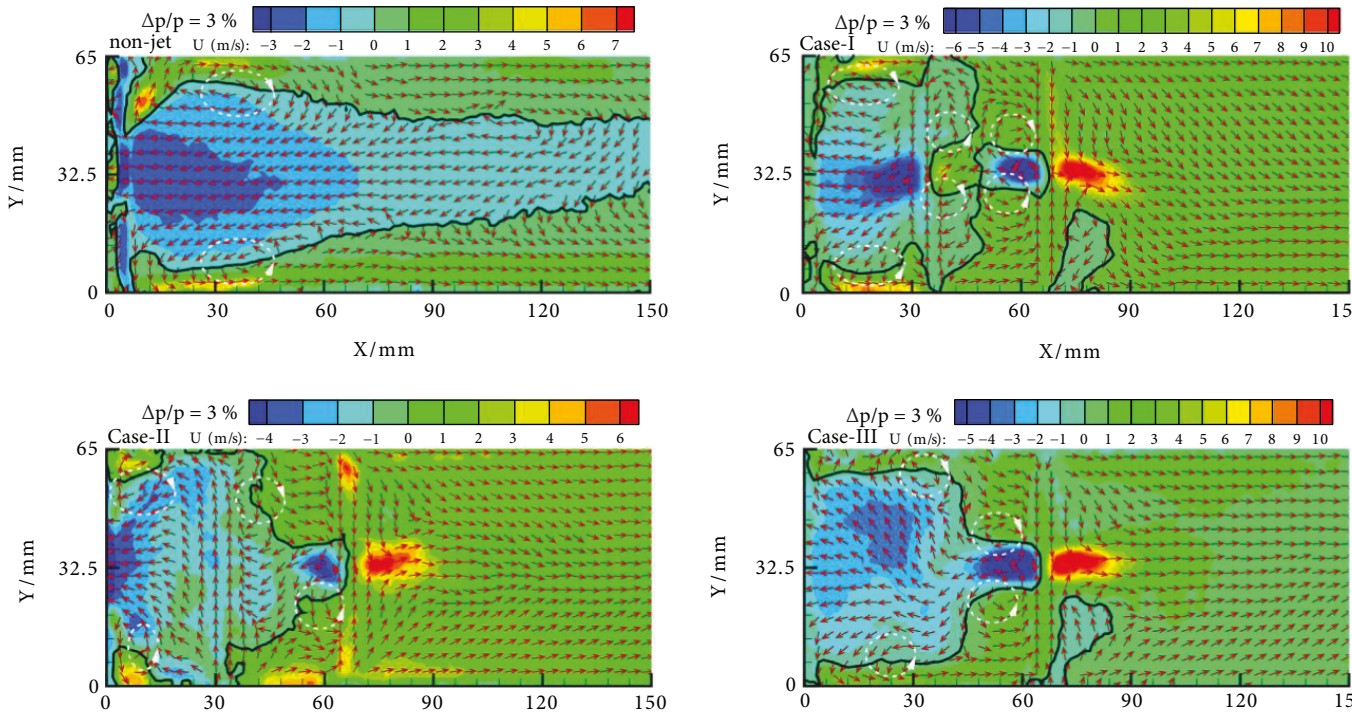

(c) Total pressure loss coefficient of 3%

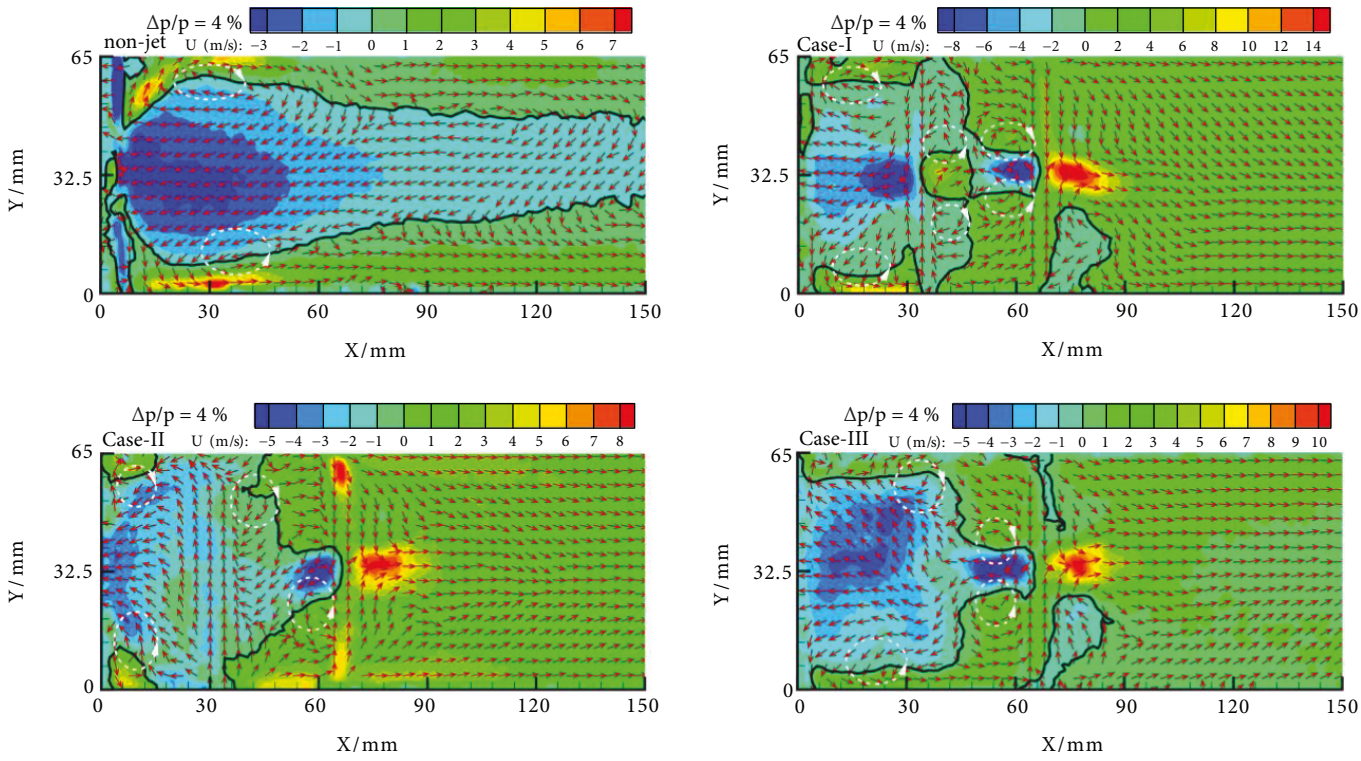

(d) Total pressure loss coefficient of 4%

Figure 3: Axial velocity contours and velocity vector plots on the $Z = 0$ mm plane.

in the Case I combustor reaches the half height of the combustor. This cuts off the central recirculation zone and forms a low-speed wake zone at the downstream joint of the primary hole jet. The wake area extends to the jet of dilution holes and cutoff at the jet of dilution holes. In addition, the local recirculation zones with opposite rotational directions are formed at the upper and lower sides of the upstream at the junction of primary holes. Compared with the combustor

model without the primary hole jet (nonjet), the height of the central recirculation zone near the outlet of the swirler significantly increases, indicating that the primary hole jet interacts with the swirler and the partial jet will enter the rich-burn zone to intensify the central recirculation zone. At the upper and lower sides of the downstream of junction of primary hole jets, the local recirculation zones with the opposite rotational directions are also formed. The formation of a local recirculation zone intensifies the momentum and mass exchange between the air flow from primary holes and the surrounding air flow, facilitating the rapid mixing in the quenching zone. As the jet depth of dilution holes reaches the half height of the combustor, the local recirculation zones with opposite rotational directions are formed at the upper and lower sides of the upstream of jet junction. Although the local recirculation zones formed in the rich-burn zone and the quenching zone occur in pair, their position and dimension are not strictly symmetrical. Although the structure of jet holes is symmetrical, the jets form an asymmetric distribution under the dome swirling. A low-speed wake area forms at the back edge of lower dilution holes but does not form around the upper orifice. The flow direction at the upper and lower sides of the lean-burn zone is asymmetric. The upper dilution hole jet dominates the air flow direction in lean-burn zone to some extent. However, the lower dilution hole jet has a higher recirculation ratio than the upper dilution hole jet. The upper primary hole jet in the Case II combustor is not on the $Z = 0$ mm plane because the upper primary hole jet has no trajectory. The jet depth of the lower primary hole jet reaches 4/5 of the height of the combustor. The jet angle is deflected by ~7° to the combustor upstream, and a local clockwise recirculation forms at the trailing edge of the jet cutoff location. Some air flow from the bottom primary holes enters the rich-burn zone and interacts with the dome swirling flow to form local recirculation zones with opposite rotational directions at the upper and lower sides of the swirler exit. Because the primary hole jet initially has a higher momentum, it gradually attenuates during the movement and the shear force between the primary hole jet and dome air flow gradually decreases. Thus, the local recirculation zones at the upper and lower sides of the swirler exit are asymmetrical. Simultaneously, the shearing action generated by the primary hole jet can form a local recirculation at the jet downstream region, intensifying the rapid mixing in the quenching zone. The central recirculation zones expand into the quenching zone and stagnate under the jet from the dilution holes. Compared with the Case I combustor, the maximum height of the central recirculation zone in the rich-burn zone increases by ~23% and the forming positions of local recirculation zones advance to the upper and lower sides of the swirler exit. The jet depth of dilution holes reaches the combustor half height and forms a counterclockwise local recirculation zone, which is at the lower side of the upstream of junction. The jet trajectory of dilution holes is deflected by ~9° to the downstream direction. The back edge of the jet does not form a low-speed wake region, and the flow direction in the lean-burn zone is substantially symmetrical. All the primary hole jets in the Case III combustor are not on the $Z = 0$ mm measuring plane. Therefore, there is no upper primary hole jet trajectory. The length of the central recirculation zone is the same as that of the Case II combustor. The central recirculation zone develops into the quenching zone and stagnates under the jet of dilution holes. However, its maximum height in the rich-burn zone decreases by ~23%, comparable to that of the Case I combustor. At the contracted positions of boundaries of the central recirculation zone, a pair of local recirculation zones with opposite directions is formed. Compared with the Case I and the Case II combustors, because the local recirculation zones in the quenching zone are formed under the shearing action of mixing pores, their positions are further backward. Therefore, the mixing capability at the downstream of the primary hole jet is weakened and the mixing distance in the quenching zone is extended. The jet depth of dilution holes reaches the half height of the combustor. Local recirculation zones with opposite rotational directions are formed at the upper and lower sides of the upstream of jet junction. A low-velocity wake region is formed at the trailing edge of dilution holes, but the trailing region behind the lower dilution holes is larger. The flow direction in the lean-burn zone is also not strictly symmetrical, and the air flow near the lower side has a higher radial velocity.

Under different total pressure loss conditions, Figure 4 shows the axial velocity distribution at different axial positions on the $Z = 0$ mm plane. The axial velocities have been normalized, and the reference value is the maximum axial velocity of the nonjet model under the condition of total pressure loss of 4%. Under different total pressure losses, the velocity distribution of the same model at each axial position is consistent. The structural characteristics of the flow field are unchanged, whereas the velocity increases with the increase in total pressure loss. It indicates that the change in total pressure loss does not affect the velocity distribution within the combustor but affects the velocity along the path. For the $X = 10$ mm plane, the axial velocity distribution of all the models exhibits an "M" shape. The velocity is in reverse within the middle range and forwards at the two sides. The height between two zero-velocity points reflects the range of the central recirculation zone. The height of the central recirculation zone in the nonjet model is ~30 mm, whereas the height of the central recirculation zone in the other three combustor models is ~51 mm. The difference in height indicates that the primary hole jet interacts with the dome swirling flow and one part of the primary hole jet forms the recirculation zone, intensifying the central recirculation zone in the rich-burn zone and increasing the height of the recirculation zone near the swirler exit. For the $X = 25$ mm plane, the axial velocity distributions in the Case III combustor and in the nonjet model are similar, both exhibiting an "M" shape. Moreover, their central recirculation zones have a similar height of ~51 mm. The height of the central recirculation zone in the Case I combustor is comparable to that in the nonjet model, but a large increase in the reverse velocity occurs in the height ranging from 20 mm to 40 mm. Combined with the flow field diagram in the Case I combustor, it can be found that the local recirculation zone formed at the leading edge of junction of primary hole jets can effectively intensify the local mixing of air flow in the central

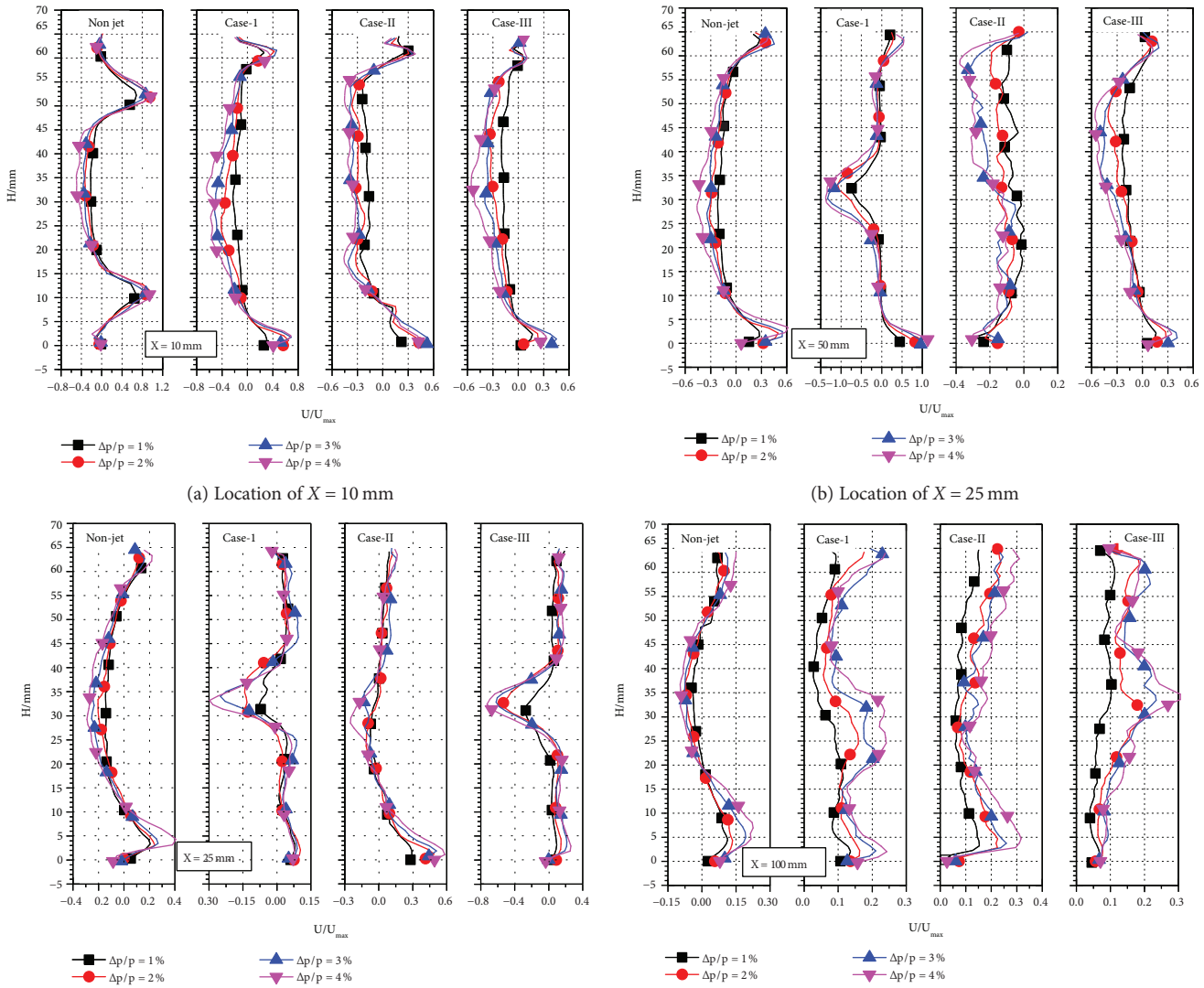

(a) Location of $X = 10$ mm

(b) Location of $X = 25$ mm

(c) Location of $X = 50$ mm

(d) Location of $X = 100$ mm

Figure 4: Axial velocity along the Y direction at different axial locations on the $Z = 0$ plane.

recirculation zone. The axial velocity in the Case II combustor exhibits a reverse velocity over the entire height range, and the reverse velocity gradually increases as the height increases. For the $X = 50$ mm location, the axial velocity distribution trend of the nonjet model remains unchanged but the height of the central recirculation zone decreases by ~5 mm compared with that on the $X = 25$ mm plane and the reverse velocity also slightly decreases, indicating that the intensity of the central recirculation zone is gradually weakened. The axial velocity distribution trends of the other three combustor models are similar, but the values of the middle reverse velocity regions are significantly different. Combined with the flow field diagrams of the three models, the reverse velocity area in the Case I combustor belongs to the wake region. Although the reverse velocity areas in the Case II and the Case III combustors belong to the central recirculation zone, the primary hole jet affects the flow field structure in the quenching zone, changing the angle of dilution hole jet and affecting the reverse velocity areas in the two cases. In addition, this phenomenon indicates that there is a greater recirculation degree for the dilution hole jet in the Case III combustor. At the location of $X = 100$ mm, the height and intensity of the central recirculation zones in the nonjet model decrease further. Moreover, the recirculation zones in the remaining three models disappeared, all showing a movement towards the downstream with forward velocities. Although the axial velocity distribution trends of the three models are slightly different, the variation extent of velocity within the height interval is not large, indicating that the primary hole jet has less effect on the flow state in the lean-burn zone.

Under the different total pressure losses of the combustor, the radial velocity distribution at different axial positions on the $Z = 0$ mm plane is shown in Figure 5. The radial velocities shown in the figure were also normalized with the reference of maximum radial velocity of the nonjet model under a total pressure loss of 4%. Under different total pressure losses, the radial velocity distribution trends for the same

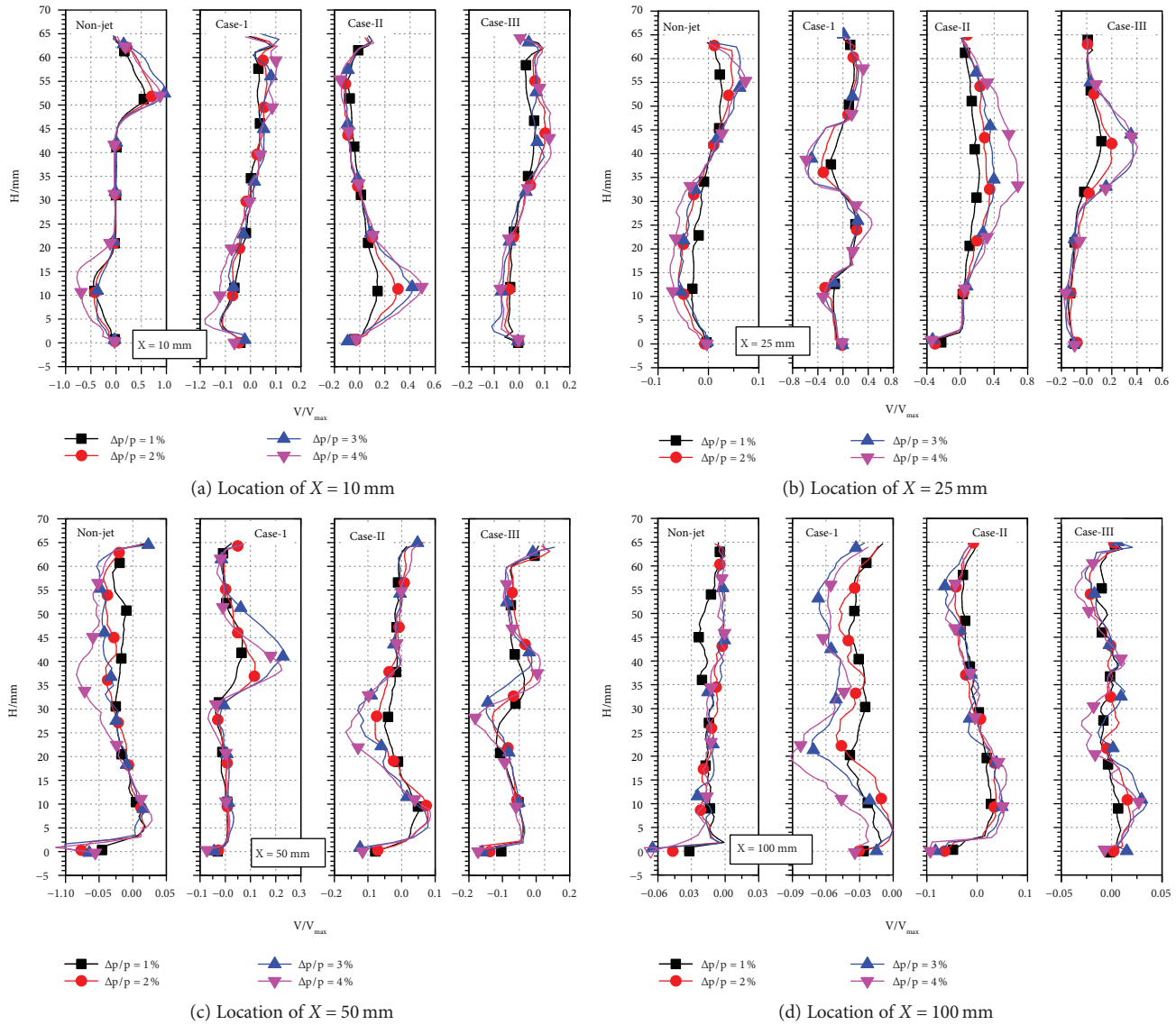

(a) Location of $X = 10$ mm

(b) Location of $X = 25$ mm

(c) Location of $X = 50$ mm

(d) Location of $X = 100$ mm

Figure 5: Radial velocity along the Y direction at different axial locations on the $Z = 0$ plane.

model at each axial position are consistent but the velocity increases with the increase in the total pressure loss, indicating that the circumferential mixing capacity in the combustor increased with the increase in total pressure loss. For the $X = 10$ mm plane, the trends of radial velocity distribution in the Case I combustor, the Case III combustor, and the nonjet model are identical. All the cases show the bimodal structure with a forward velocity at the upper side and a reverse velocity at the lower side, but the nonjet model has a higher peak velocity. The distribution trend shows that the jet obtained from the primary holes interacts with the dome-rotating air flow. Therefore, some air flow from the primary holes strengthens the dome energy dissipation when it enters the rich-burn zone and intensifies the mixing process in the rich-burn zone. Although the radial velocity distribution in the Case II combustor also shows a bimodal structure, its velocity distribution is opposite to those of the other three combustor models. Compared with the upper reverse velocity, the lower forward velocity has a higher peak value. Because the higher initial momentum of the primary hole jet gradually decreases during the movement, the shearing action also exhibits a gradual decay. This leads to an inconsistent local recirculation intensity of the rich-burn zone in the Case II combustor, and the lower local recirculation zone has a higher intensity. After combining the axial velocity distribution on the $X = 10$ mm plane in the Case II combustor as shown in Figure 4, it was found that the peak axial velocity appears on two sides and the velocity near the height center is lower than those of the other two combustor models due to the formation of local recirculation zones at the upper and lower sides. The results indicate that at the position, although the local recirculation was intensified, the intensity of the center recirculation zone is slightly weakened because the directions of radial velocity and dome air flow are opposite. On the $X = 25$ mm plane, the radial velocity distribution of the nonjet model still maintains the same bimodal

structure as that at the swirler exit but the peak velocity significantly decreases. The other three combustor models show completely inconsistent structural characteristics. The Case I combustor has a distinct bimodal distribution near the combustor height center because of the formation of a pair of local recirculation zones with opposite rotational directions. For the Case II combustor, only the single-hole jet from the bottom primary hole appears on the measured plane and it has a high momentum. Therefore, a distribution of forward velocity is manifested under the jet dragging. Simultaneously, the distributed region of forward velocity is basically consistent with the distributed region of forward velocity given by the nonjet model. Then, the central recirculation zone was intensified. As a result, the boundary of the central recirculation zone in the Case II combustor in Figure 3 is rapidly expanded after the contraction. In addition, combined with the axial velocity distribution on the $X = 25$ mm plane in the Case II combustor (Figure 4), the axial velocity in the central recirculation zone is intensified when the region has a radial velocity direction consistent with that of the nonjet model. However, the axial velocity in the central recirculation zone decreases in the region where the velocity is opposite. Therefore, the interaction between the primary hole jet and dome swirling flow will affect the characteristics of the central recirculation zone. The central recirculation zone is intensified as the air flow develops along the direction that facilitates the tangential momentum generated by the swirler. For the opposite direction, the central recirculation zone is weakened. The velocity distribution trends in the Case III combustor and nonjet model are basically the same, exhibiting a bimodal structure. However, the peak velocity in the Case III combustor is higher and the peak position is more close to the combustor height center with a slightly higher positive peak. Although the Case III combustor does not show the trajectory of the primary hole jet on its $Z = 0$ mm measured plane, the radial velocity of air flow in the rich-burn zone is generally consistent with the direction of the nonjet combustor model. The tangential momentum is enhanced, leading to the increase on the central recirculation zone. For the $X = 50$ mm plane, although the radial velocity distribution of the nonjet model still exhibits a bimodal structure, its distribution is opposite to that in the rich-burn zone and the velocity decreases further. This is because the centrifugal force generated by the swirler significantly attenuated. This is insufficient to overcome the entrainment to the air flow generated by the central low-pressure area and local recirculation zone. Therefore, the central recirculation zone cannot continue to expand. In the Case I combustor and the Case III combustor, the bimodal structural characteristics appear at the two sides of the combustor height because both the cases have a pair of local recirculation zones with opposite rotational directions. The Case II combustor only forms a local recirculation zone at the lower side of the combustor height center. Under the entrainment action by the local recirculation zone, the air flow at the upper side moves towards the recirculation zone and the entrainment is stronger when the air flow is closer to the recirculation zone. Therefore, although the radial velocity distribution in the Case II combustor has a bimodal structure as well, all the peak velocities are below the combustor height center, while the velocity above the height center is mainly manifested as the reverse velocity. On the $X = 100$ mm plane, although the radial velocity distribution trends of the four models are different to a certain degree, the velocities are very low. Combined with Figure 4, the axial velocity dominates within the lean-burn zone, determining the overall flow state.

The axial velocity distribution curves obtained from the $Z = 0$ mm measured plane to the combustor height center ($Y = 32.5$ mm) are shown in Figure 6. The red dashed line in the figure is the dividing line, and the selected points are the centers of the primary holes and dilution holes. The axial velocity of the nonjet model appears as a reverse velocity along the path. Simultaneously, the velocity along the path first rapidly increases and then gradually decreases. The axial velocity in the Case I combustor slowly increases in the rich-burn zone and rapidly increases before the primary holes. Simultaneously, compared with the nonjet model, the axial velocities along the path are higher, indicating that the primary hole jet cuts off the development of the central recirculation zone and increases the recirculation intensity in the rich-burn zone, especially for the local recirculation at the jet leading edge. In the quenching zone, a local high-velocity gradient region is formed at the trailing edge of junction because the primary hole jets converge at the center. Simultaneously, a strong shearing action is formed when the primary hole jets interact with the dilution hole jets and a low-speed wake region is formed at the leading edge of junction for the dilution hole jets. Thus, the axial velocity distribution in the quenching zone exhibits a sinusoidal distribution trend. In the lean-burn zone, a local high-velocity gradient region appears at the trailing edge of the junction point for the dilution hole jets. In the region, the axial velocity first rapidly increases and then gradually decreases, eventually becoming stable. The axial velocity distributions in the Case II combustor and the Case III combustor are basically consistent. Both of them are stably developed with reverse velocities in the rich-burn zone and quenching zone, suddenly increase before the dilution holes, and have identical cutoff points for the reverse velocity. However, the reverse velocity in the Case II combustor gradually decreases in front of the $X = 20$ mm plane. This indicates that the central recirculation zone in both the cases was developed to the quenching zone and cut off by the dilution hole jet but the strength of the central recirculation zone in the Case II combustor is weakened before the $X = 20$ mm plane. In the lean-burn zone, the development of both the center recirculation zones first rapidly increases and then gradually decreases and finally stably develops along the downstream direction.

It can be observed from the abovementioned studies that the variation in total pressure loss mainly affects the velocity of air flow and slightly affects the flow field structure in the combustor. Therefore, only the flow field structures on the $Z = -15.5$ mm measured planes under the design point state ($\Delta p/p = 4\%$) were analyzed. Figure 7 shows the flow field structure on the $Z = -15.5$ mm plane in the model combustor with different structural parameters of the primary holes. For the nonjet model, the central recirculation zone still exists, indicating that the central

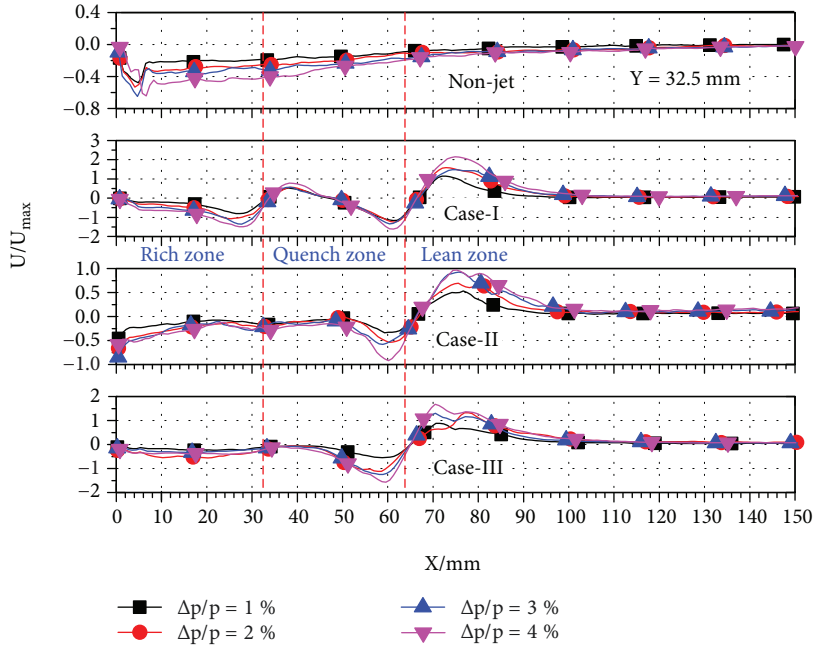

Figure 6: Axial velocity along the X direction at $Y = 32.5$ mm on the $Z = 0$ mm plane.

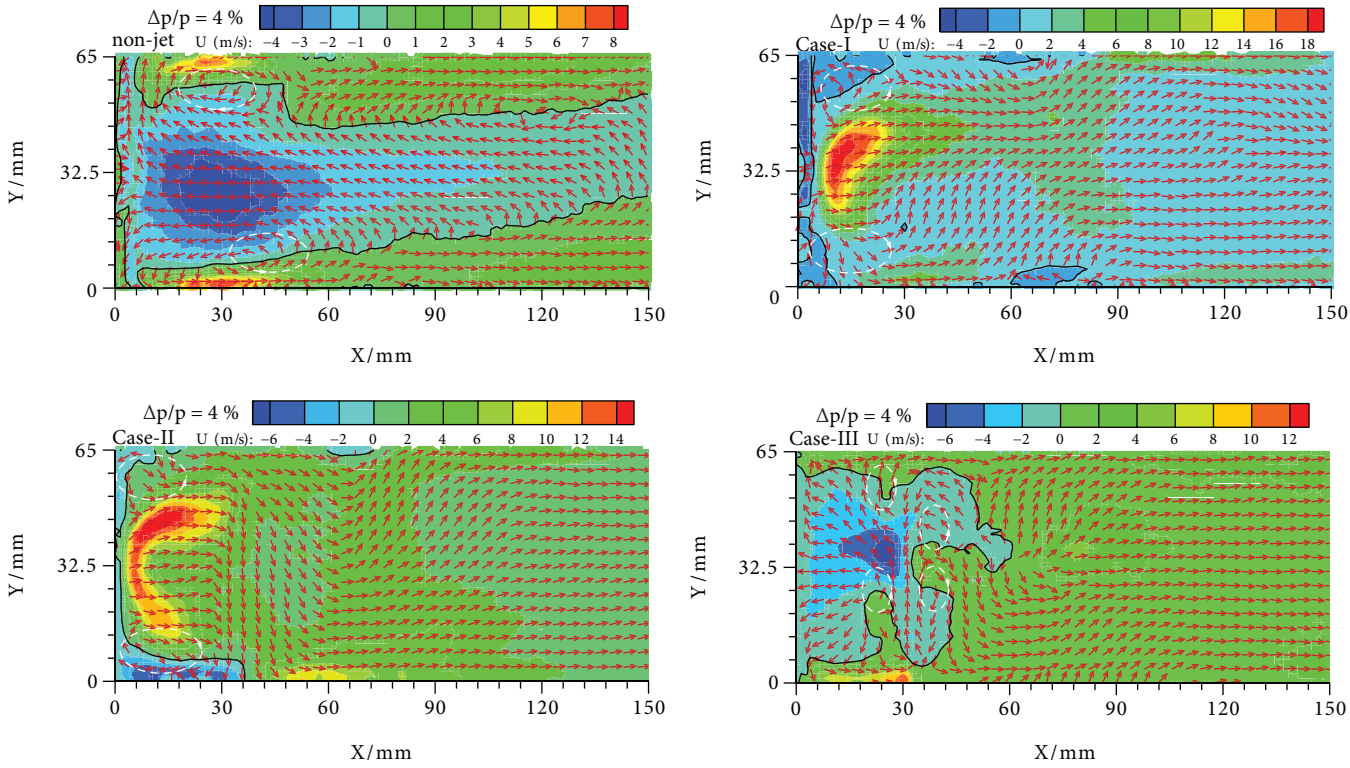

Figure 7: Axial velocity contours and velocity vector plots on the $Z = -15.5$ mm plane.

recirculation zone is not a 2D planar structure but has three-dimensional (3D) structural characteristics. Although similar to the $Z = 0$ mm plane, a local recirculation with an opposite rotational direction is formed at the highest point of boundary of the central recirculation zone. However, the lower boundary exhibits a gradually upward inclination, while the upper boundary exhibits a sudden contraction after a gradual increase. The central recirculation zone in the Case I combustor disappears, and a higher axial velocity is formed at the swirler exit, exhibiting a larger

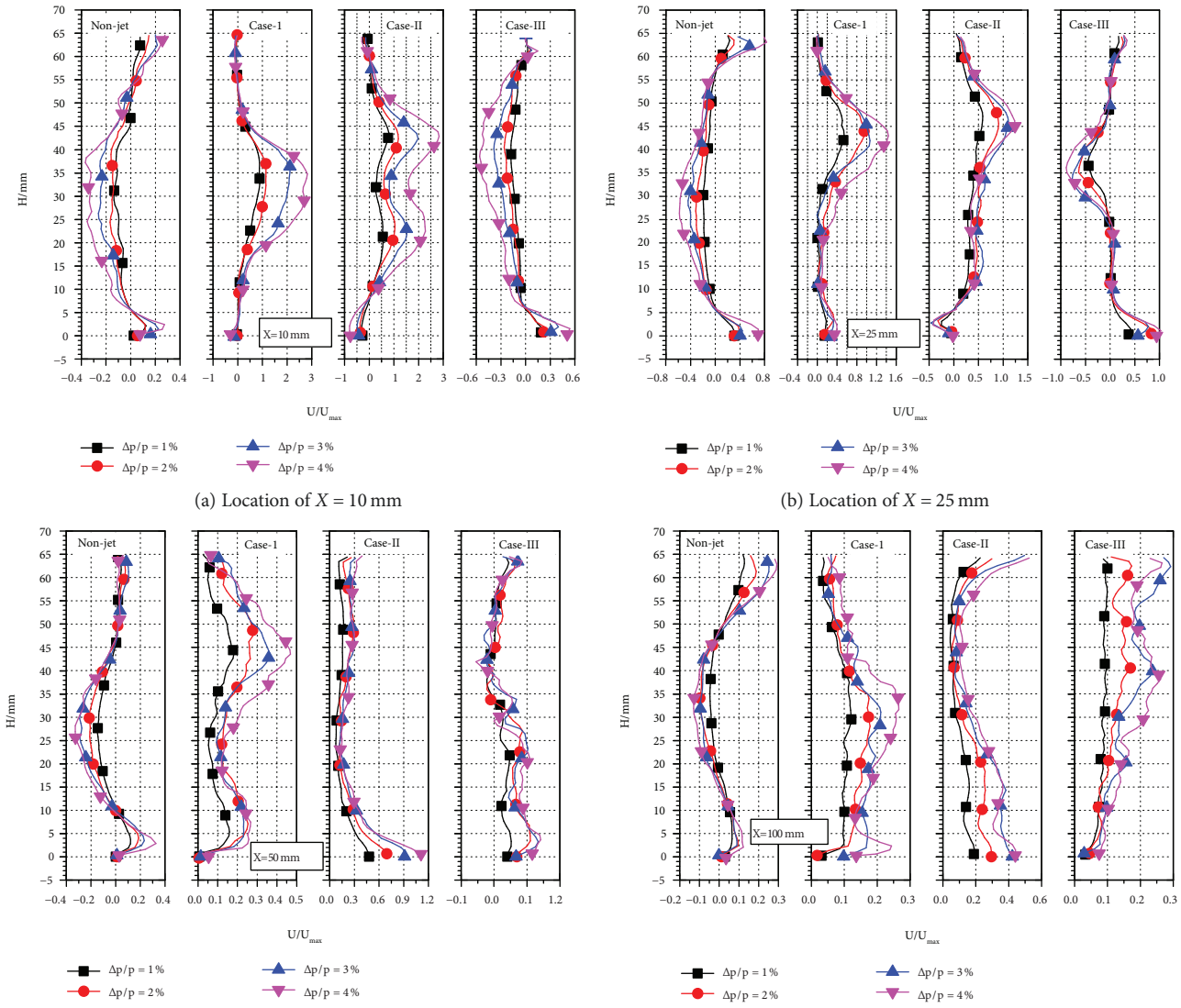

(a) Location of $X = 10$ mm

(b) Location of $X = 25$ mm

(c) Location of $X = 50$ mm

(d) Location of $X = 100$ mm

FIGURE 8: Axial velocity along the Y direction at different axial locations on the $Z = -15.5$ mm plane.

velocity gradient. Under the shear action caused by a high axial velocity, a pair of local recirculation zones with opposite rotational directions is formed at the upper and lower sides of the swirler exit. In addition, the entire shooting area exhibits a flow with forward velocity and no regions with large velocity gradients appear. In addition, a significant radial velocity occurs near the $X = 30$ mm plane which is at the position of the primary hole jet. However, when it moves to the location of half height of the combustor, it quickly merges into the mainstream and moves downstream within the mainstream. It can be inferred from these phenomena that the radial velocity is generated by the entrainment vortex generated by the adjacent primary hole jets. It cannot initiate the local recirculation zone but moves downstream under the dragging force of axial air flow because it does not have a higher momentum to form a strong shearing action with the high-speed axial air flow. However, the formation of an entrainment vortex inhibits the development of the local central recirculation zone and changes the flow field structure in the combustor. Similar to the Case I combustor, except for the high axial velocity gradient at the swirler exit and the occurrence of the local recirculation zone at the corners, the entire shooting region in the Case II combustor exhibits a flow with forward velocity and without regions of large velocity gradients. Simultaneously, a significant radial velocity occurs near the position of the primary hole jet. However, the radial velocities in the Case I combustor and Case II combustor are opposite and the height of radial velocity in the Case II combustor is basically equal to the height of the combustor. The difference indicates that the entrainment vortex formed between the primary hole jets in the Case II combustor has a greater height. In the Case III combustor, the diameter of primary holes and the spacing between adjacent holes are smaller ($D = 4$ mm, $S = 27$ mm). Therefore, the measured plane is

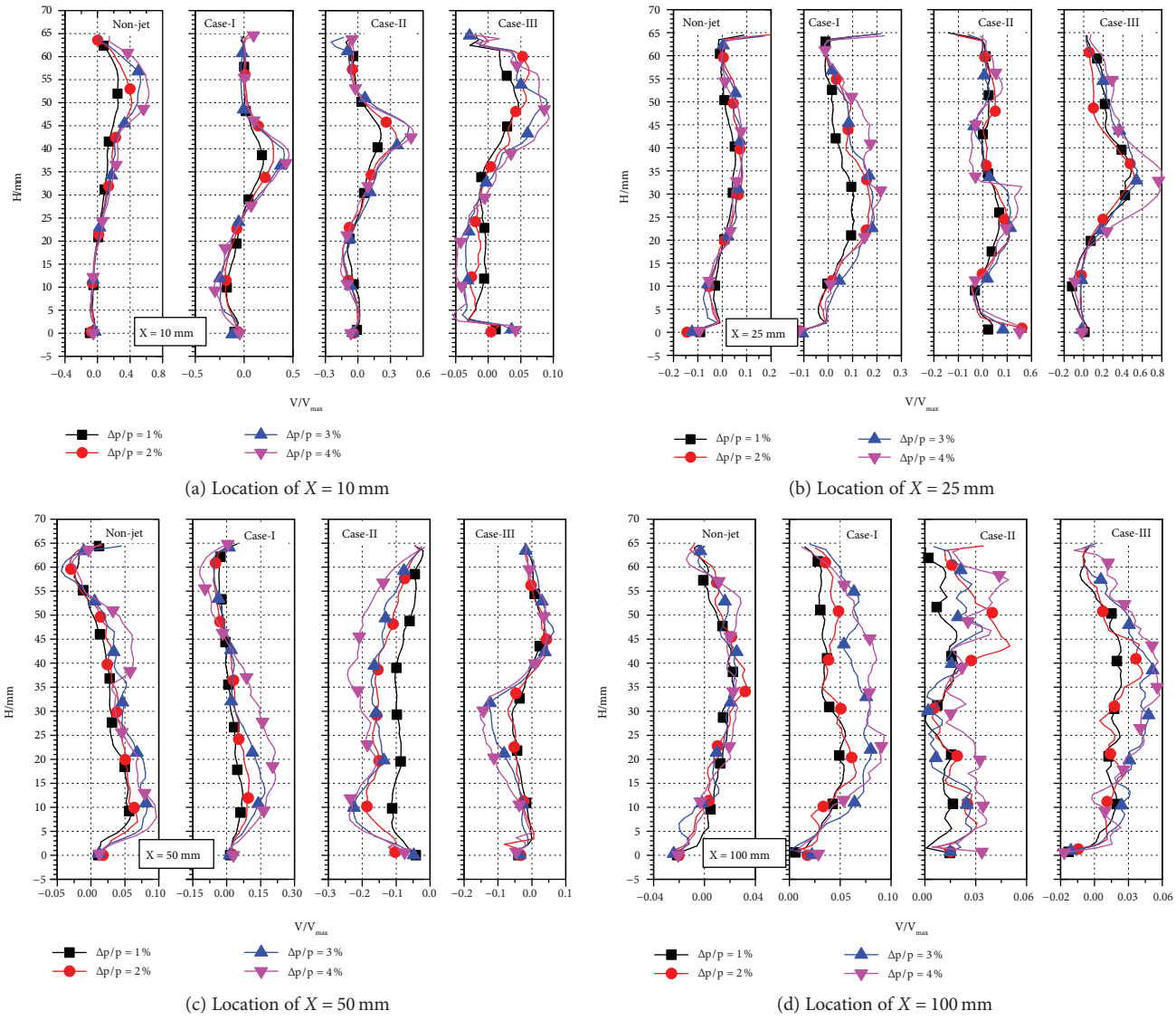

(a) Location of $X = 10$ mm

(b) Location of $X = 25$ mm

(c) Location of $X = 50$ mm

(d) Location of $X = 100$ mm

FIGURE 9: Radial velocity along the Y direction at different axial locations on the $Z = -15.5$ mm plane.

at the edge of the primary holes. Although the jet core region does not appear on the measured plane, a jet trajectory with a higher radial velocity ($V_{max} = 30$ m/s) appears on the plane due to the rapid expansion of jet flow, indicating that the jet flow cuts off the central recirculation zone. Moreover, under the strong shearing action, two groups of local recirculation zones with opposite rotational directions are formed before and after the jet flow. Some jet flow enters the rich-burn zone and intensifies the central recirculation zone, thus increasing the height of the central recirculation zone. It was again proved that the disappearance of the central recirculation zones in the Case I combustor and Case II combustor is closely related to the entrainment vortex formed between the jet holes.

The axial velocity distributions at different axial positions on the $Z = -15.5$ mm plane under different total pressure losses is shown in Figure 8. Under different total pressure losses, the velocity distribution trends for the same model at each axial position are consistent. However, the velocity increases with the increase in total pressure loss. It is further verified that the flow field structure characteristics will not vary with the variation in total pressure loss, indicating that the flow is in a self-modeling state. For the $X = 10$ mm plane, the velocity distribution trend of the nonjet model is basically consistent with that of the Case III combustor. This is characterized by the reverse velocity distribution in the central recirculation zone and the forward velocity distribution outside the recirculation zone. However, the height of the central recirculation zone in the Case III combustor is improved by at least 10%. Although both the Case I combustor and the Case II combustor exhibit the distribution of forward velocity, the Case II combustor exhibits a bimodal distribution which is an "M" structure. At the $X = 25$ mm plane, there are still central recirculation zones in the nonjet model combustor and the Case III combustor. However, the height of the

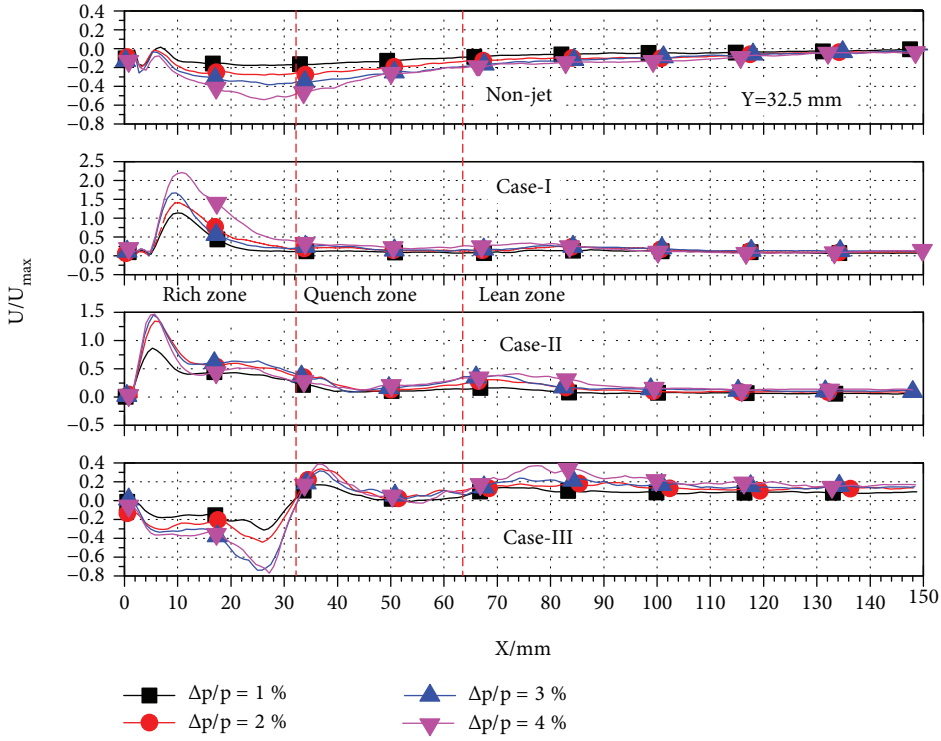

Figure 10: Axial velocity along the X direction at $Y = 32.5$ mm on the $Z = -15.5$ mm plane.

central recirculation zone in the Case III combustor decreases by ~40%, while the peak velocity significantly increases. The Case I combustor and Case II combustor still have the forward velocity distribution, but the velocity distribution trends in the two cases are slightly different. On the $X = 50$ mm plane, the height of the central recirculation zone of the nonjet model is ~20% lower than that of the rich-burn zone. For the axial velocity distribution in the Case III combustor, it can be vaguely observed that it has a bimodal distribution with the reverse velocity at the upper side and forward velocity at the lower side, while the peak value of reverse velocity is extremely low. The distribution indicates that in the height range of position, the recirculation zone is asymmetrical and the recirculation intensity is lower. Although the axial velocities in the Case I combustor and Case II combustor both exhibit forward distribution, the position of the peak velocity in the Case I combustor is above the center of the combustor, whereas the peak velocity in the Case II combustor is near the combustor lower wall. Moreover, the peak velocities in the two cases are both lower than the corresponding velocities in the rich-burn zone. At the $X = 100$ mm plane, the nonjet model combustor still has a central recirculation zone, while the reverse velocity significantly decreases in the central recirculation zones. All the other three model combustors exhibit a distribution of forward velocity with a small variation over the height of the combustor. The entrainment vortex formed between the adjacent primary hole jets in the Case I combustor and Case II combustor suppresses the development of the central recirculation zone. Simultaneously, because the primary hole jets with different structures lead to a large difference in the entrainment vortex structure, it has a significant effect on the velocity distribution in the combustor. Especially, it has an extremely significant effect on the flow states in the rich-burn zone and the quenching zone. The results will cause different penetrations of local air flow. Therefore, the mixing effect and residence time of local air flow are different as well.

The radial velocity distribution for different axial positions on the $Z = -15.5$ mm plane under different total pressure loss conditions is shown in Figure 9. At the $X = 10$ mm plane, although the radial velocity distribution trends of the four models are consistent, the radial peak velocities in the Case I combustor and the Case II combustor are much lower than their axial velocities and the ratio between the two is ~0.2. The results indicate that the axial momentum completely dominates, eventually leading to the failure in establishing the central recirculation zones. At the $X = 25$ mm plane and the $X = 50$ mm plane, the tangential momentum generated by the swirler rapidly decays. Therefore, the effects of entrainment vortex and primary hole jet on the velocity distribution are very obvious. The primary hole jet can intensify the local recirculation and enhance the mixing ability of local air flow. Further, combined with the axial velocity distribution as shown in Figure 8, it was found that the radial velocity generated by the entrainment vortex and the axial velocity in the combustor are mutually constrained. The radial air flow suppresses the penetrating ability of axial air flow, while the axial air flow limits the permeating ability of the radial air flow, finally resulting in the uneven distribution of local air mixing and residence time in the

combustor. At the $X = 100$ mm plane, the tangential momentum generated by the swirler and the entrainment vortex formed between the jet holes significantly decreased. The radial velocity is low, and the variation is small over the entire height range, which indicates that the axial air flow completely dominates.

The axial velocity distribution curves on the $Z = -15.5$ mm plane and along the path passing the center of the combustor are shown in Figure 10. Along the path direction, the axial velocity of the nonjet model combustor first increases and then gradually decreases. From the perspective of the 3D structure, the recirculation zones first expand and then shrink. The axial velocity developments along the paths in the Case I combustor and the Case II combustor are developments with a forward velocity that first rapidly increases, then gradually decreases, and finally achieves a steady forward velocity. However, the location of the peak velocity in the Case I combustor has a lag of ~65% compared with that in the Case II combustor and the peak velocity significantly increases. The different structures and intensities of the entrainment vortex would affect the development of the velocity along the path. The variation in the axial velocity in the rich-burn zone in the Case III combustor is similar to that of the nonjet model combustor. However, the reverse velocity rapidly increases before the primary holes and the peak velocity is higher than the nonjet model combustor. The primary hole jet in the Case III combustor effectively intensifies the central recirculation. In its quenching, the axial velocity undergoes a development with forward velocity that increases rapidly, gradually decreases, and finally becomes steady.

It is not difficult to determine from the above PIV test results that the primary hole jet significantly affects the flow field structure in the combustor. In the quenching zone, the flow is uneven due to the formation of local recirculation zones. This will impose a certain effect on the residence time within the quenching zone. Moreover, the residence time within the quenching zone is a key factor affecting the formation of NO_x, the mixing effect, and the combustion efficiency in the quenching zone. It is essential to understand the effects of the primary hole jet on the residence time within the quenching zone. The result of 2D PIV measurement has numerous data points in the measured plane, which can be written as an $M \times N$ matrix. The residence time within the quenching zone is mainly determined by the axial velocity distribution in its interval. Therefore, the axial velocity distribution within the quenching zone can be used to estimate the average residence time. For the calculation method, refer to formula (1). In the formula, $U_{M\times N}$ is the $M \times N$ matrix composed of the axial velocity at each point in the quenching zone, M is the number of data points along the axial direction, N is the number of data points along the radial direction, $\bar{U}_M$ is the average value of axial velocity of each row in the matrix, u is the axial velocity of each point in the matrix, l is the length of the quenching zone, t_M is the average residence time for each row in the matrix, and $\bar{t}$ is the average dwelling time within the quenching zone.

$$U_{M\times N} = \begin{bmatrix} u_{11} & \cdots & u_M \\ \vdots & \ddots & \vdots \\ u_{M1} & \cdots & u_{MN} \end{bmatrix} \Rightarrow \bar{U}_M = \begin{bmatrix} \frac{1}{n}\sum_1^n u_1 \\ \vdots \\ \frac{1}{n}\sum_1^n u_M \end{bmatrix} \Rightarrow t_M = \begin{bmatrix} \frac{l}{\bar{U}_1} \\ \vdots \\ \frac{l}{\bar{U}_M} \end{bmatrix} \Rightarrow \bar{t} = \frac{1}{m}\sum_1^m t. \quad (1)$$

For the $Z = 0$ mm plane and the $Z = -15.5$ mm plane, Figure 11 shows the average residence time within the quenching zone for the three model combustors under the conditions of different total pressure loss. As the total pressure loss increases, the average residence time within the quenching zone is shortened but the shortening extent gradually decreases. For the same total pressure loss, the average residence time on the $Z = -15.5$ mm plane is ~73% shorter than that on the $Z = 0$ mm plane. In addition, the Case II combustor has the shortest average residence time on both the $Z = 15.5$ mm and $Z = 0$ mm planes. On the $Z = 0$ mm plane, the average residence time of the Case II combustor has 65% and 68% reductions compared with those of the Case I combustor and the Case III combustor, respectively, and the average residence time on the $Z = 15.5$ mm plane was shortened by 64% and 70%, respectively. The shortening in residence time indicates that the structure of the primary holes and total pressure loss significantly affect the average residence time in the quenching zone and the residence times in different planes are inconsistent. When the primary holes are located at the half height of the combustor, the interconnected structure of primary holes and the increase in the flow rate of the partial single-hole jet can significantly shorten the residence time within the quenching zone.

The flow in the combustor has obvious 3D characteristics. Therefore, the measurement results of axial planes cannot reflect the circumstantial characteristics of the flow field. To clarify the effects of the primary hole jet on the combustor circumferential flow, the PIV measurement results of circumstantial planes with axial distances of 20 mm, 32.5 mm, 48 mm, and 63.5 mm from the swirler exit are shown in Figures 12–15.

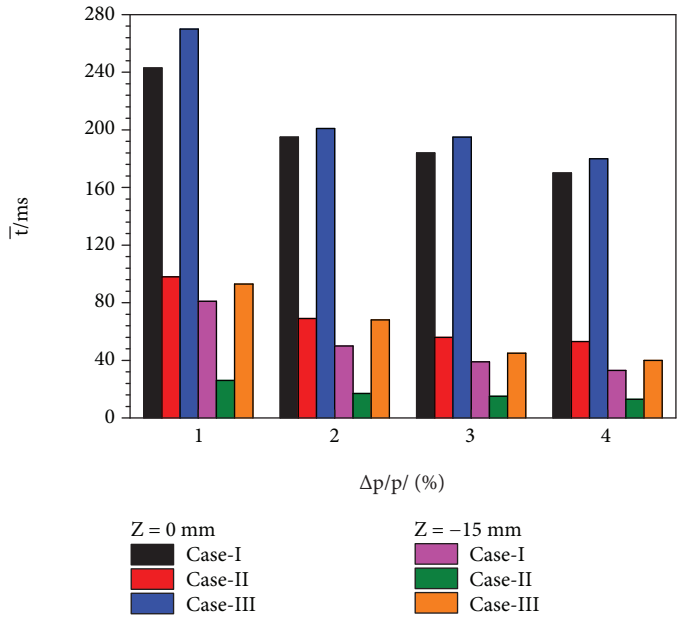

Figure 11: Residence time for the quenching zone on the $Z = 0$ mm plane and $Z = -15.5$ mm plane.

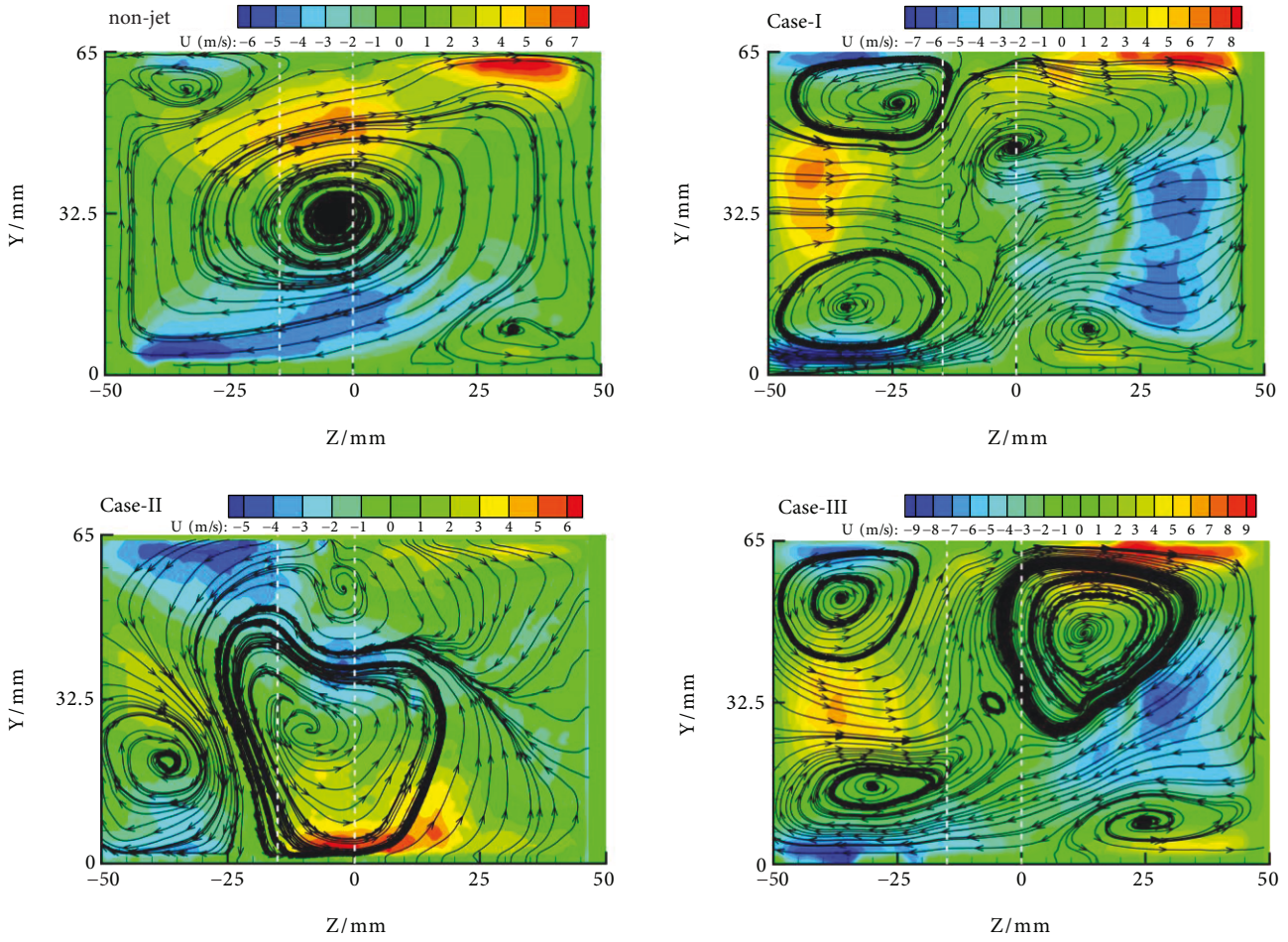

Figure 12: Axial velocity contours and streamline in the plane of $X = 20$ mm.

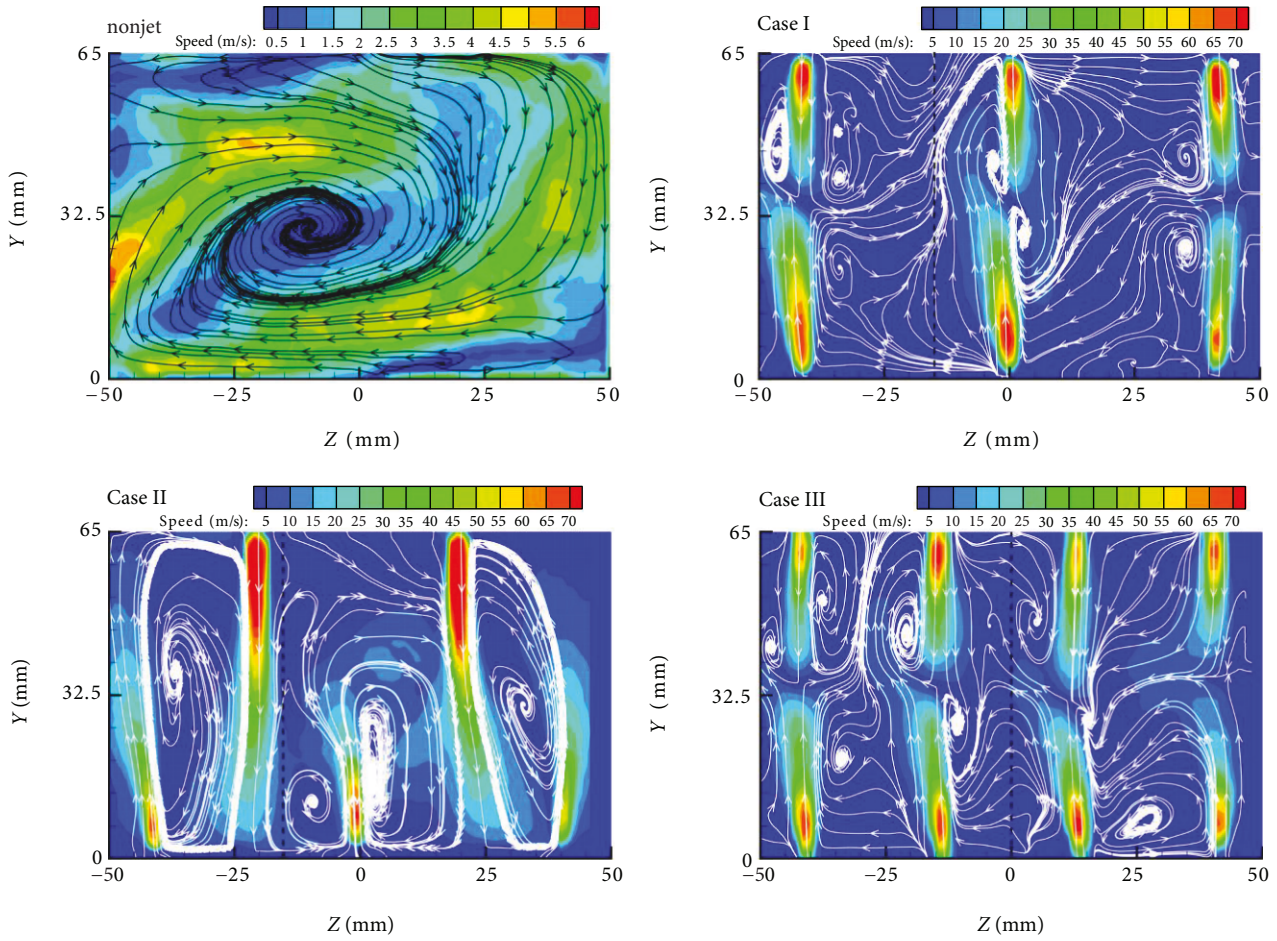

Figure 13: Resulting velocity contours and streamline on the $X = 32.5$ mm plane.

As shown in Figure 12, in the nonjet model combustor, the air flow rotates and expands from the center to the periphery because the air flow passing through the swirler has a strong tangential momentum. This can generate a centrifugal force to cause the air flow to rotate. The rotational direction is related to the initial direction of the tangential momentum. This is determined by the swirler structure and exhibits a clockwise direction. In addition, because the air flow rapidly expands after entering the combustor through the swirler, an angular vortex is formed at the corner and has a rotational direction opposite to the main air flow. When the hole jet is introduced, its flow field structure is completely changed and recirculation zones are formed in several circumstantial local regions, thus increasing the local mixing for air flow along the combustor circumferential direction. However, the locations, rotational directions, and dimensions of local recirculation zones are different under the primary hole jets with different structures. Such differences affect the characteristics of central recirculation zones. The correlation between the $Z = 0$ mm plane and the $Z = -15.5$ mm plane is illustrated by the measurement results. The locations of the $Z = 0$ mm plane and the $Z = -15.5$ mm plane are indicated by the white dashed lines. At the passing location of the $Z = 0$ mm plane, the local recirculation zones exist at the upper sides in the Case I combustor and the Case III combustor. Although the dimensions of the local recirculation zone are inconsistent, the rotational direction of the recirculation zone is the same as the mainstream rotational direction of the nonjet model combustor. Simultaneously, the direction of air flow at the lower side is also the same as the mainstream direction of the nonjet model combustor. This helps to increase the mainstream tangential momentum.

Therefore, the intensity of the central recirculation zone increases. This is also the reason why the Case III combustor has no primary hole jet on the $Z = 0$ mm plane but its central recirculation zone is still intensified. The upper and lower sides in the Case II combustor both have local recirculation simultaneously. Although the dimension of the recirculation zone at the lower side is large, their rotational directions are opposite to that of the mainstream. This will weaken the tangential momentum of the mainstream and then decrease the intensity of the central recirculation zone. Therefore, on the $Z = 0$ mm plane, there is a case where the boundaries of the initial recirculation zone shrink and the reverse velocity at center height decreases. Simultaneously, it is also the reason why the radial velocity distribution trend at the $X = 10$ mm plane is opposite to that of the reference model. At the passing location of the $Z = -15.5$ mm plane, local recirculation zones exist at both the upper and lower sides in the Case I

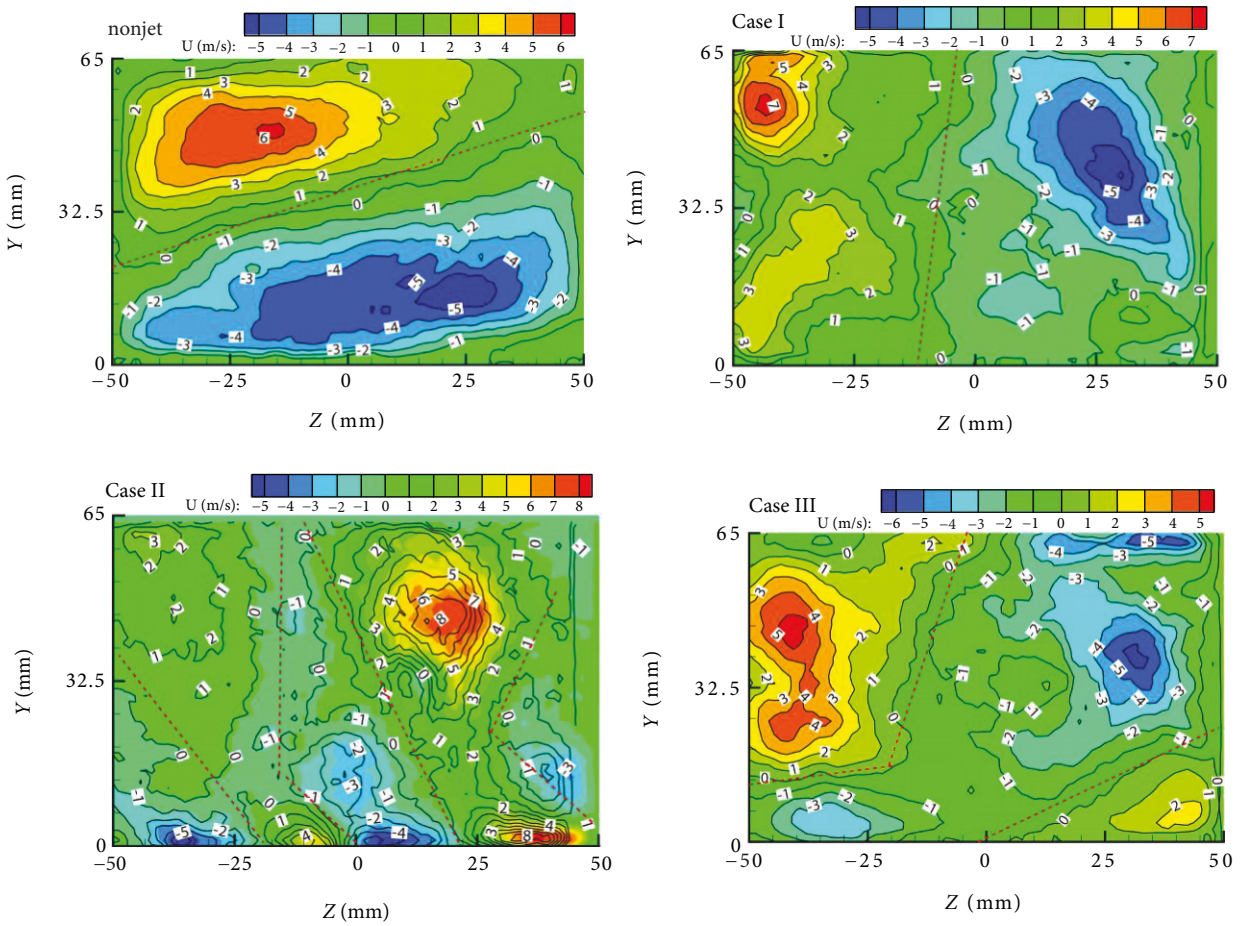

Figure 14: Axial velocity contour on the $X = 48$ mm plane.

combustor. The rotational direction of the upper recirculation zone is opposite to that of the mainstream, while that at the lower side is the same as that of the mainstream. However, in general, only the air flow near the lower wall has the same direction with that of the mainstream and the air flow in the remaining height ranges is perpendicular or opposite to that of the mainstream. The direction of overall air flow in the Case II combustor is opposite to that of the mainstream air flow. The air flow perpendicular or opposite to the direction of the main air flow will significantly weaken the tangential momentum of the main flow, thereby suppressing the development of the central recirculation zone. When the tangential momentum of the mainstream air flow significantly decreases and the axial momentum quickly dominates, the local central recirculation zone will be suppressed. That is why the central recirculation zone is absent on the $Z = -15.5$ mm plane in the Case I combustor and the Case II combustor. The passing air flow maintains the same flow direction as that of the mainstream air flow, thereby increasing the tangential momentum of the mainstream air flow and strengthening the central recirculation zone.

The combined velocity contour and streamline diagram of the circumstantial plane with an axial distance of the $X = 32.5$ mm plane in the combustor are shown in Figure 13. The black dashed lines in the Case I combustor and the Case II combustor represent the passing positions of the $Z = -15.5$ mm plane, while that in the Case III combustor represents the passing position of the $Z = 0$ mm plane. Although the streamline direction of the nonjet model combustor is the same as that of the $X = 20$ mm plane, it clearly shows that the airflow accumulates from the periphery to the center. The tangential momentum generated by the swirler significantly decreases. Thus, the momentum is insufficient to maintain the continual expansion of the central recirculation zone. Therefore, the central recirculation zone enters a gradual shrinking phase. However, because of the presence of a central negative pressure zone, the circumstantial air flow moves towards the center and generates a tangential momentum. This can maintain the downstream development of the central recirculation zone. For the Case I combustor and the Case II combustor, the jet depth of the primary holes almost reaches the half height of the combustor. Because of the interaction between the primary hole jet and dome swirling flow, the trajectory of the primary hole jet is not perpendicular and can form local recirculation zones between the adjacent two primary holes, namely, an entrainment vortex. The entrainment vortex intensifies the transfer and exchange of momentum and mass between the primary hole jet and the surrounding mixed air flow and promotes the rapid mixing

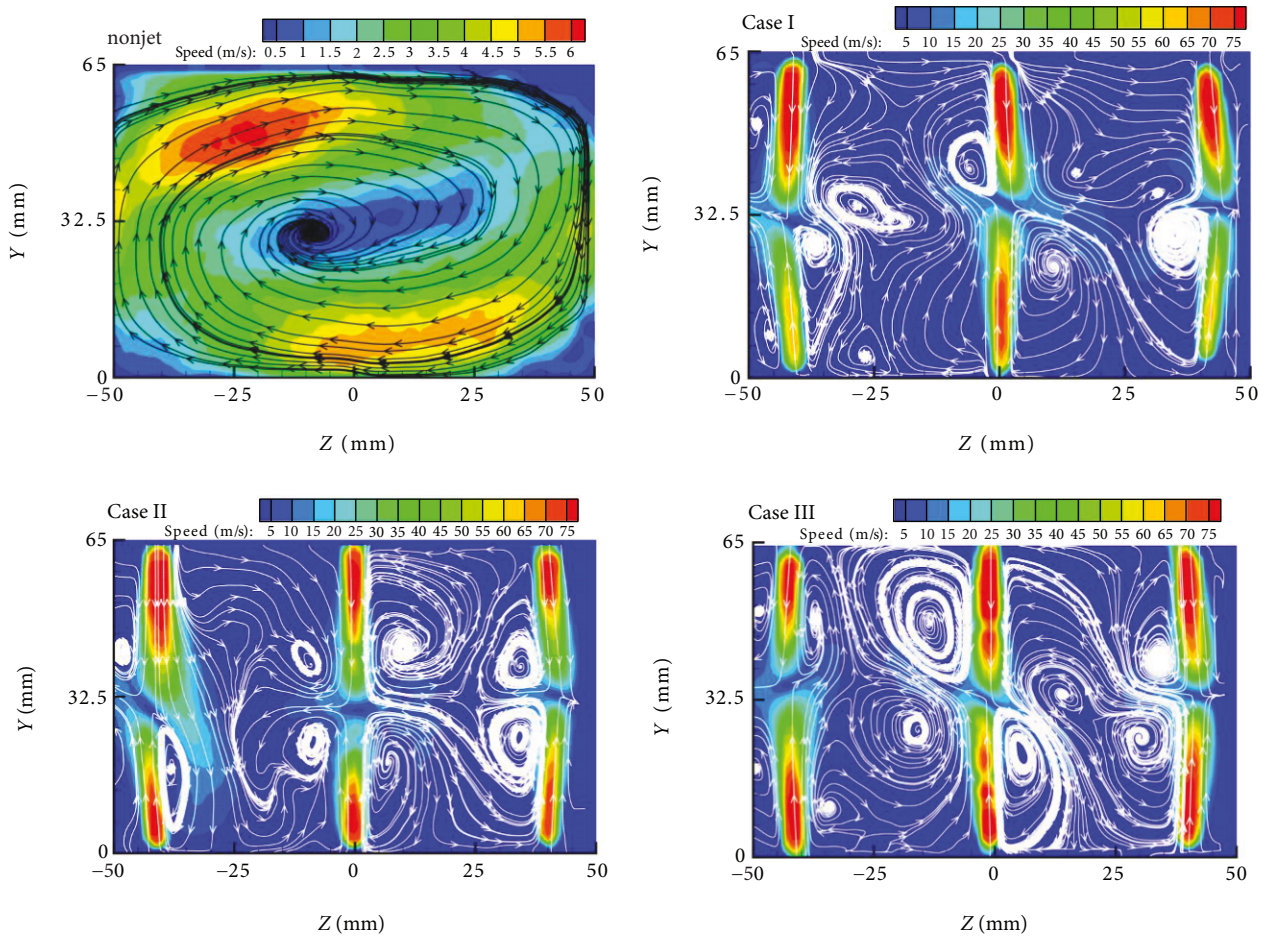

Figure 15: Resulting velocity contours and streamline on the $X = 63.5$ mm plane.

of the jet along the circumferential direction. The Case III combustor has more vortexes between adjacent jets owing to the smaller spacing between the holes, and the interaction between vortexes further promotes the rapid mixing capability of the jet on the plane. For the Case II combustor, the upper primary holes have a jet depth of ~25% higher than that of the bottom primary holes, indicating that a larger hole can produce a higher jet penetration depth. Simultaneously, entrainment vortexes with opposite rotational directions are formed between each pair of the upper and bottom adjacent primary holes and the height of the entrainment vortex substantially covers the entire combustor. The formation of the entrainment vortex facilitates the mixing of the combustor circumferential air flow. Simultaneously, it has a significant effect on the flow state of the air flow.

Therefore, the jet obtained from the primary holes with different structures will lead to a difference in the mixing performance and flow field structure. In addition, for the $Z = -15.5$ mm plane in the Case I combustor and the Case II combustor, radial air flows exist in the vertical direction, where the radial air flow in the Case I combustor moves from the bottom to the top and reaches over the half height of the combustor. The radial air flow in the Case II combustor moves from the top to the bottom and substantially covers the height of the entire combustor. Therefore, it was confirmed that the radial air flow on the measuring plane of the $Z = -15.5$ mm plane in the Case I combustor and the Case II combustor results from the entrainment vortex between the jets obtained from the adjacent primary holes. Simultaneously, under the action of the entrainment vortex, the direction of air flow movement at this position is generally perpendicular or opposite to the mainstream direction of the nonjet model combustor. This can suppress the development of the central recirculation zone and further lead to the rapid shrinkage of the central recirculation zone. Therefore, no central recirculation zone was observed at the $Z = -15.5$ mm measured plane in the Case I combustor and the Case II combustor. In comparison, the $Z = 0$ mm plane in the Case III combustor is also in the acting range of the entrainment vortex but the tangential momentum was intensified and the development of the central recirculation zone was strengthened because the direction of the air flow is basically the same as the mainstream direction of the nonjet model combustor. In addition, combined with Figure 13, it was observed that the rotational direction of the entrainment vortex in each region is the same as that of the corresponding local recirculation zone and the moving direction of the entrainment air flow around them is also substantially consistent. It can be concluded that the formation of an entrainment vortex is the main reason for the formation a

circumferential local recirculation zone in the rich-burn zone. Simultaneously, the local recirculation zone interacts with the swirling flow produced by the swirler, thus affecting the local characteristics of the central recirculation zone.

The axial velocity gradient cloud chart of the circumstantial plane with an axial distance of the $X = 48$ mm plane is shown in Figure 14. The red dashed line was used to separate the regions with forward and reverse velocities. The upper region of the nonjet model combustor exhibits a forward velocity, whereas the lower region exhibits a reverse velocity. The velocity distribution in the Case I combustor is a left-right division with a forward velocity gradient on the left and a reverse velocity gradient on the right. Generally, the velocity distribution in the Case II combustor appears as an alternation between the regions with forward velocity and reverse velocity. The Case III combustor is mainly characterized by a forward velocity area distributed in the upper left and lower right and a reverse velocity area in the middle.

Simultaneously, compared with the nonjet model combustor, the model with the introduction of the primary hole jet has a smaller local range with a large velocity gradient, indicating that the interaction between the primary hole jet and dome swirling air flow can effectively increase the mixing capacity in the combustor and shorten the mixing distance between fuel and air. In addition, a comparison between combustor models with three different structures of primary holes shows that the large-velocity gradient region in the Case III combustor is large, whereas the Case I combustor and the Case II combustor only have large-velocity gradients in localized small regions. For the quenching zone in the Case III combustor, the rapid mixing ability becomes poorer and the mixing distance increases, indicating that the jet obtained from primary holes has a significant effect on the mixing capability of air flow in the quenching zone. The increase in the number of primary holes and decrease in the momentum of the single-hole jet are not conducive to the rapid mixing in the quenching zone. Therefore, a reasonable optimization of the structure of primary holes is the key factor to achieve rapid mixing in the quenching zone.

The combined velocity and flow diagram of a circumferential plane with an axial distance of the $X = 63.5$ mm plane is shown in Figure 15. The central recirculation zone in the nonjet model combustor is still maintained. The jet depth of dilution holes in the other three combustor models reaches the half height of the combustor. The jet trajectory is not completely vertical to each other and forms the local recirculation zone. It is shown that the swirling air flow still exists and can interact with the jet obtained from the dilution holes. Although the forming positions of local recirculation zones between the three model combustors are slightly different, in general, the rotational direction of the local recirculation zones on the corresponding positions is completely consistent. The results indicate that the effect of the primary hole jet on the flow field structure is still present but the effect significantly decreases compared with those of the rich-burn zone and quenching zone. In addition, compared with the other two model combustors, the Case III combustor has a larger entrainment vortex between adjacent jets and the formation position of the optimum mixing effect on the quenching zone is more lagged.

4. Conclusions

In this study, the flow characteristics of a single-dome rectangular RP-3 kerosene fueled in the RQL combustor with high temperature rise were investigated. Under ambient temperature and pressure, the axial positions of primary holes and the structural parameters of the dilution holes are unchanged. The 2D PIV technology was used to perform the cold flow field measurement on the combustor equipped with the primary holes of different structures. Moreover, the effect of the primary hole structure on the flow characteristics of the combustor was evaluated. With the change in the total pressure loss of the combustor, the flow field structure characteristics of the combustor are basically unchanged. However, the velocity along the air flow path in the combustor increases and the average residence time in the quenching zone is shortened. The variations in the array mode of the primary holes and diameter have a more significant effect on the combustor flow characteristics, especially for the structure of the central recirculation zone, the distribution of the local recirculation zones in the rich-burn zone and quenching zone, and the average residence time in the quenching zone. The stagger arrangement of primary holes can significantly shorten the average residence time in the quenching zone. On the circumferential plane passing though the center of the primary holes, the characteristics of the entrainment vortex formed by the primary holes with different structures are clearly different. The flow characteristics of the entrainment vortex determine the positions and flow states of the local recirculation zones in the rich-burn zone and affect the local parts of the central recirculation zone. When the rotational direction of local recirculation is the same as that of the mainstream at the combustor dome, the local central recirculation is intensified, and conversely, it is weakened.

Data Availability

The data used to support the findings of this study are available from the corresponding author upon request.

Conflicts of Interest

The authors declare that they have no conflicts of interest.

Acknowledgments

This work was supported by "the National Natural Science Foundation of China" (no. 51476077).

References

[1] H. C. Mongia, "Engineering aspects of complex gas turbine combustion mixers part I: high ΔT," in *49th AIAA Aerospace Science Meeting including the New Horizons Forum and Aerospace Exposition*, Orlando, FL, USA, 2011.

[2] H. C. Mongia, "Engineering aspects of complex gas turbine combustion mixers part II: high T3," in *49th AIAA Aerospace Science Meeting including the New Horizons Forum and Aerospace Exposition*, Orlando, FL, USA, 2011.

[3] H. C. Mongia, "Engineering aspects of complex gas turbine combustion mixers part III: 30 OPR," in *9th Annual International Energy Conversion Engineering Conference*, San Diego, CA, USA, 2011.

[4] H. C. Mongia, "Gas turbine combustion design, technology and research - current status and future direction," in *33rd AIAA/ASME/ASEE Joint Propulsion Conference and Exhibit*, Seattle, WA, USA, 1997.

[5] H. C. Mongia, "Aero-thermal design and analysis of gas turbine combustion systems - current status and future direction," in *34th AIAA/ASME/ASEE Joint Propulsion Conference and Exhibit*, Cleveland, OH, USA, 1998.

[6] D. W. Bahr, "Technology for the design of high temperature rise combustors," *Journal of Propulsion and Power*, vol. 3, no. 2, pp. 179–186, 1987.

[7] K. D. Brundish, M. N. Miller, and L. C. Morgan, "Variable fuel placement injector development," in *ASME Turbo Expo 2003, Paper 2003-GT-38417*, pp. 425–443, Atlanta, GA, USA, 2003.

[8] Y. Sugiyama and R. Takamuta, "Research and development of a 1600°C-level combustor with high heat release rate," in *ISABE 95-7099, Proceedings of Twelfth International Symposium on Air Breathing Engines*, pp. 1077–1087, Reston, VA, USA, 1995.

[9] R. Friend, "Turbine engine research in the United States Air Force," in *2001 IEEE Aerospace Conference Proceedings (Cat. No.01TH8542)*, vol. 7, pp. 7–3178, Big Sky, MT, USA, 2001.

[10] D. M. Zhu, R. A. Miller, and D. S. Fox, "Thermal and environmental barrier coating development for advanced propulsion engine systems," in *NASA/TM-2008-215040*, 2008.

[11] S. A. Mosier and R. M. Pierce, *Advanced Combustor Systems for Stationary Gas Turbine Engines, Phase I: Review and Preliminary Evaluation*, Contract 68-02-2136, FR-11405, Final Report. U. S Environmental Protection Agency, 1980.

[12] A. S. Novick, D. L. Troth, and J. Notardonato, "Multifuel evaluation of rich/quench/lean combustor," *Mechanical Engineering*, vol. 105, no. 5, pp. 1–8, 1982.

[13] G. S. Samuelsen, J. Brouwer, M. A. Vardakas, and J. D. Holdeman, "Experimental and modeling investigation of the effect of air preheat on the formation of NO_X in an RQL combustor," *Heat and Mass Transfer*, vol. 49, no. 2, pp. 219–231, 2013.

[14] R. C. McKinney, D. Sepulveda, W. Sowa, and A. K. Cheung, "The Pratt & Whitney TALON X low emissions combustor: revolutionary results with evolutionary technology," in *45th AIAA aerospace sciences meeting and exhibit*, Reno, Nevada, 2007.

[15] A. S. Feitelberg and M. A. Lacey, "The GE rich-quench-lean gas turbine combustor," in *International Gas Turbine and Aero-engine Congress & Exhibition*, Orlando, FL, USA, 1997.

[16] T. G. van, J. J. Hwang, M. K. Kim, and K. Y. Ahn, "Feasibility study of ultra-low NOX gas turbine combustor using the RML combustion concept," *Journal of Mechanical Science and Technology*, vol. 30, no. 12, pp. 5749–5757, 2016.

[17] A. M. Mellor, *Design of Modern Turbine Combustors*, Academic Press, London, UK, 1990.

[18] A. H. Lefebvre, *Gas Turbine Combustion*, CRC Press, New York, NY, USA, 2010.

[19] S. J. Shanbhogue, Y. S. Sanusi, S. Taamallah, M. A. Habib, E. M. A. Mokheimer, and A. F. Ghoniem, "Flame macrostructures, combustion instability and extinction strain scaling in swirl-stabilized premixed CH_4/H_2 combustion," *Combustion and Flame*, vol. 163, pp. 494–507, 2016.

[20] C. T. Chong and S. Hochgreb, "Spray flame structure of rapeseed biodiesel and jet-A1 fuel," *Fuel*, vol. 115, pp. 551–558, 2014.

[21] C. T. Chong and S. Hochgreb, "Spray flame study using a model gas turbine swirl burner," *Applied Mechanics and Materials*, vol. 316-317, pp. 17–22, 2013.

[22] M.-K. Kim, J. Yoon, S. Park, M.-C. Lee, and Youngbin Yoon, "Effects of unstable flame structure and recirculation zones in a swirl-stabilized dump combustor," *Applied Thermal Engineering*, vol. 58, no. 1-2, pp. 125–135, 2013.

[23] J. Chen, Y. Wang, H. Liu, and Y. Weng, "Experimental study of flow characteristics of enhanced biogas lean premixed nozzle of micro gas turbine by PIV," *Applied Thermal Engineering*, vol. 121, pp. 90–102, 2017.

[24] Y. Yan, Y. Liu, J. Li, and W. Cai, "Investigations of combustion performance in LPP combustor," *Journal of Applied Fluid Mechanics*, vol. 10, no. 5, pp. 1271–1282, 2017.

[25] M. Schroll, U. Doll, and G. Stockhausen, "Flow field characterization at the outlet of a lean burn single sector combustor by laser-optical methods," *Journal of Engineering for Gas Turbines and Power*, vol. 139, no. 011503, pp. 1–9, 2017.

[26] I. Boxx, C. Slabaugh, P. Kutne, R. P. Lucht, and W. Meier, "3 kHz PIV/OH-PLIF measurements in a gas turbine combustor at elevated pressure," *Proceedings of the Combustion Institute*, vol. 35, no. 3, pp. 3793–3802, 2015.

[27] L. G. Becker, H. Kosaka, B. Böhm et al., "Experimental investigation of flame stabilization inside the quarl of an oxyfuel swirl burner," *Fuel*, vol. 201, pp. 124–135, 2017.

[28] C. D. Richards and G. S. Samuelsen, "The role of primary jet injection on mixing in gas turbine combustion," *Symposium (International) on Combustion*, vol. 23, no. 1, pp. 1071–1077, 1991.

[29] C. D. Richards and G. S. Samuelsen, "The role of primary jets in the dome region aerodynamics of a model can combustor," *Journal of Engineering for Gas Turbines and Power*, vol. 114, no. 1, pp. 20–26, 1992.

[30] B. Mohammad, S. M. Jeng, and M. G. Andac, "Influence of the primary jets and fuel injection on the aerodynamics of a prototype annular gas turbine combustor sector," *Journal of Engineering for Gas Turbines and Power*, vol. 133, no. 1, article 011505, 2011.

[31] S. Gogineni, D. Shouse, C. Frayne, J. Stutrud, and G. Sturgess, "Combustion air jet influence on primary zone characteristics for gas-turbine combustors," *Journal of Propulsion and Power*, vol. 18, no. 2, pp. 407–416, 2002.

[32] A. Elkady, S. M. Jeng, and H. C. Mongia, "The influence of primary air jets on flow and pollutant emissions characteristics within a model gas turbine combustor," in *44th AIAA Aerospace Sciences Meeting and Exhibit*, Reno, Nevada, 2006.

[33] D. W. Bar and W. J. Dodds, *Gas Turbine Combustor Design*, Academic Press Limited, Waltham, MA, USA, 1990.

[34] E. V. Kartaev, V. A. Emel'kin, M. G. Ktalkherman, V. I. Kuz'min, S. M. Aul'chenko, and S. P. Vashenko, "Analysis of mixing of impinging radial jets with crossflow in the regime of counter flow jet formation," *Chemical Engineering Science*, vol. 119, pp. 1–9, 2014.

[35] J. Chen, J. Li, L. Yuan, and G. Hu, "Flow and flame characteristics of a RP-3 fuelled high temperature rise combustor based on RQL," *Fuel*, vol. 235, pp. 1159–1171, 2019.

[36] F. Vashahi, S. Lee, and J. Lee, "Experimental analysis of the swirling flow in a model rectangular gas turbine combustor," *Experimental Thermal and Fluid Science*, vol. 76, pp. 287–295, 2016.